



HAL
open science

Thick interfaces coupling technique for weakly dispersive models of waves

Martin Parisot

► **To cite this version:**

Martin Parisot. Thick interfaces coupling technique for weakly dispersive models of waves. 2024. hal-04452924

HAL Id: hal-04452924

<https://hal.science/hal-04452924>

Preprint submitted on 12 Feb 2024

HAL is a multi-disciplinary open access archive for the deposit and dissemination of scientific research documents, whether they are published or not. The documents may come from teaching and research institutions in France or abroad, or from public or private research centers.

L'archive ouverte pluridisciplinaire **HAL**, est destinée au dépôt et à la diffusion de documents scientifiques de niveau recherche, publiés ou non, émanant des établissements d'enseignement et de recherche français ou étrangers, des laboratoires publics ou privés.

Thick interfaces coupling technique for weakly dispersive models of waves

Martin Parisot*¹

¹Team CARDAMOM, Inria Bordeaux Sud-Ouest, 200 Avenue de la
vieille tour, 33405 Talence cedex

February 12, 2024

Abstract

The primary focus of this work is the coupling of dispersive free-surface flow models through the utilization of a thick interface coupling technique. The initial step involves introducing a comprehensive framework applicable to various dispersive models, demonstrating that classical weakly dispersive models are encompassed within this framework. Next, a thick interface coupling technique, well-established in hyperbolic framework, is applied. This technique enables the formulation of unified models across different subdomains, each corresponding to a specific dispersive model. The unified model preserves the conservation of mechanical energy, provided it holds for each initial dispersive model. We propose a numerical scheme that preserve the projection structure at the discrete level and as a consequence is entropy-satisfying when the continuous model conserve the mechanical energy. We perform a deep numerical analysis of the waves reflected by the interface. Finally, we illustrate the usefulness of the method with two applications known to pose problems for dispersive models, namely the imposition of a time signal as a boundary condition or the imposition of a transparent boundary condition, and wave propagation over a discontinuous bathymetry.

1 Introduction

The present research is dedicated to the coupling of dispersive models of free surface flows. While dispersive models, such as the Peregrine equations [41] or Green-Naghdi equations [23], are essential for wave propagation at the free surface, they exhibit less robustness compared to shallow water equations in various scenarios. Specifically, in dry fronts, most numerical strategies for solving dispersive models encounter stability issues. Furthermore, weakly non-linear models (such as Boussinesq-like equations) are not well-posed in these regions. Instabilities also occurs in areas

*martin.parisot@inria.fr

with steep variations in bathymetry (non-Lipschitz bathymetry), where dispersive models lack well-posed solutions [30], or with vertical roofs [11, 19]. Additionally, understanding the boundary conditions of dispersive models remains incomplete, although some research is paving the way [25, 32, 33, 39]. In practical applications, the imposition of flow at the boundary requires source terms on the layers around it [5, 44]. In all these configurations, the shallow water model proves to be more robust, and various strategies exist. Also for modeling breaking waves, one strategy involves local use of the shallow water model, capable of dissipating energy through shocks [26]. The primary goal of this work is to couple dispersive models with shallow water equations to address the mentioned challenges. Similarly, we will explore the coupling between weakly non-linear and fully non-linear dispersive models. The main advantage of this coupling is its computational efficiency compared to simulations using the fully non-linear model throughout the entire domain. Specifically, in regions where water depth is sufficiently large and remains relatively constant, weakly non-linear models yield similar results to fully dispersive models [27] and they are more cost-effective since the matrix used for resolving dispersive terms remains constant throughout the simulation.

This research is grounded in the reformulation of dispersive models as a hyperbolic model projected onto a linear subspace. Subsequently, we employ a coupling strategy commonly used for hyperbolic models [21, 22]. In §2.1, a comprehensive description of the continuous framework to which we refer is provided, and in §2.2, we demonstrate that several classical dispersive models can be expressed in this form. The unified model, which accomplishes the coupling of models within the continuous framework, is presented in §2.3. This model, parametrized by a spatial function θ , reverts to one of the previously mentioned models when θ takes the value of 0 or 1. If the unified model is derived from two mechanical energy-preserving models and uses a single hyperbolic operator, it also preserves mechanical energy.

For the models considered in this work, this is notably the case for the coupling between the Green-Naghdi and shallow water equations, and for the coupling between the Yamazaki and shallow water equations. Moving on to §3, we consider the discrete counterpart of the previous models. The strategy does not rely on domain decomposition with transmission conditions but involves discretizing the continuous unified model. This approach allows the definition of intermediate areas where $\theta \in]0, 1[$, making the coupling smoother. This strategy is generally referred to as thick interface coupling. Applying the numerical strategy proposed in [40], §3.1 describes a numerical scheme that preserve the projection structure at the discrete level and as a consequence ensures the dissipation of discrete mechanical energy when verified at the continuous level. Finally, in §4, several numerical experiments have been conducted to study the behavior of the coupling.

2 Continuous framework

2.1 General setting of the projected hyperbolic models

We focus on models, called later projected hyperbolic models, under the form

$$(1) \quad \partial_t \begin{pmatrix} H \\ U \end{pmatrix} + A(H, U) \nabla \begin{pmatrix} H \\ U \end{pmatrix} = - \begin{pmatrix} 0 \\ \Psi \end{pmatrix}$$

where the state variables $H(t, x) \in \mathbb{R}^{d_H}$ and $U(t, x) \in \mathbb{R}^{d_U}$ will be respectively called the potential and the velocity unknowns. We assume that the matrix $A(H, U) \in M_{d_H+d_U}(\mathbb{R})$ is diagonalisable so that omitting the right hand side, the model is hyperbolic. The right-hand side of (1), which will be referred to as the dispersive source term $\Psi(t, x)$, is not explicitly defined but is constructed to ensure that the velocity variable satisfies a relation

$$(2) \quad L_H(U) = 0$$

with $L_H: \mathbb{R}^{d_U} \mapsto \mathbb{R}^{d_c}$ and $0 \leq d_c \leq d_U$ called the constraint, possibly parametrized by the potential variable H . We make the assumption that the constraint is a linear function of the velocity variable U , and we represent the set of functions \mathbf{U} satisfying $L_H(\mathbf{U}) = 0$ as \mathbb{A}_H . The dispersive source term Ψ is assumed to belong to \mathbb{A}_H^\perp , the orthogonal complement of the set of admissible functions with respect to the inner product $\langle \bullet, \bullet \rangle_H: \left((L^2)^{d_U} \right)^2 \mapsto \mathbb{R}$, i.e. for any $\Phi \in \mathbb{A}_H^\perp$ and any $\mathbf{U} \in \mathbb{A}_H$, we have

$$(3) \quad \langle \mathbf{U}, \Phi \rangle_H = 0.$$

Finally, we incorporate into the model the initial conditions $H(0, x) = H^0(x)$ and $U(0, x) = U^0(x) \in \mathbb{A}_{H^0}$.

Assume the hyperbolic operator exhibits an entropy structure, meaning there exists a pair of entropy-flux functions (E, G) dependent on the state variables (H, U) such that for sufficiently regular state variables, the relation

$$(4) \quad (\nabla_{H,U} E)^T A = (\nabla_{H,U} G)^T$$

holds true. Note that this condition is a common feature in numerous hyperbolic models, as discussed in references such as [6, 20]. Moreover, assume that the entropy $E(H, U) = \mathcal{P}(H) + \mathcal{K}(H, U)$ can be decomposed into a potential part dependent solely on the potential variables $\mathcal{P}(H)$ and a kinetic part defined through a weight function $v: \mathbb{R}^{d_H} \mapsto \mathbb{R}_+$, i.e. $\mathcal{K}(H, U) = \frac{v(H)}{2} |U|^2$. Consequently, the set of admissible functions $\mathbb{A}_H = \{ \mathbf{U} \in L^2(v(H)) \mid L_H(\mathbf{U}) = 0 \}$ forms a linear subspace of $L^2(v(H)) := \{ \mathbf{V} \mid \int_{\mathbb{R}^d} |\mathbf{V}|^2 v(H) dx < \infty \}$. If the inner product used to define the dispersive source term is the same as that used to define the kinetic energy, i.e., $\langle \mathbf{V}^1, \mathbf{V}^2 \rangle_H = \int_{\mathbb{R}^d} v(H) \mathbf{V}^1 \cdot \mathbf{V}^2 dx$, then \mathbb{A}_H^\perp also forms a linear subspace of L^2_H and the two spaces are in direct sum, i.e. $L^2_H = \mathbb{A}_H \oplus \mathbb{A}_H^\perp$. Furthermore, the entropy $E(H, U)$ serves as an energy for the projected hyperbolic model (1).

Proposition 1. *If there exists a pair of entropy-flux functions (E, G) satisfying the condition (4), and the dispersive source term Ψ satisfies the orthogonality condition (3) with the inner product associated to the kinetic energy $\langle \mathbf{V}^1, \mathbf{V}^2 \rangle_H = \int_{\mathbb{R}^d} v(H) \mathbf{V}^1 \cdot \mathbf{V}^2 dx$, then the sufficiently regular solutions of the projected hyperbolic model (1) satisfy to the following energy conservation law*

$$\partial_t \int_{\mathbb{R}^d} E(H, U) dx = 0.$$

Proof. Multiplying (1) by $\nabla_{H,U} E$, we have

$$\nabla_{H,U} E \cdot \left(\partial_t \begin{pmatrix} H \\ U \end{pmatrix} + A(H, U) \nabla \begin{pmatrix} H \\ U \end{pmatrix} + \begin{pmatrix} 0 \\ \Psi \end{pmatrix} \right) = \partial_t E + \nabla \cdot G + \nabla_U E \cdot \Psi.$$

Given that the entropy E depends on the velocity variable only through the kinetic energy, we have $\nabla_U E = v(H)U$. Therefore, by integrating over the spatial variable, the last term vanishes as $U \in \mathbb{A}_H$ and $\Psi \in \mathbb{A}_H^\perp$. \square

Some can be interesting by the flux of energy $\mathcal{G}(H, U, \Psi)$ to write a local energy conservation for (1), i.e.

$$(5) \quad \partial_t E + \nabla \cdot \mathcal{G} = 0.$$

Specifically, the conservation of energy is ensured when this flux remains continuous. It's crucial to note that this flux \mathcal{G} isn't solely the hyperbolic flux G since the dispersive source term, or more precisely the associated Lagrange multiplier, can also contribute. Refer to §2.2 for illustrative instances. The orthogonality property (3) bears a striking resemblance to the duality observed between the pressure gradient and divergence-free velocity fields in incompressible fluid mechanics. More precisely, a significant number of models adhering to the projection structure outlined in §2.1 are reductions of the water wave equations [14].

2.2 Some examples of projected hyperbolic models

To illustrate the concept, this section provides examples of classical models that satisfy the projection structure defined in §2.1. To explicitly define a model within the family of projected hyperbolic models as outlined in §2.1, it is necessary to specify the potential variable H , the velocity variable U , the hyperbolic operator A , the linear constraint $L_H(\mathbf{V})$, and the inner product $\langle \mathbf{V}^1, \mathbf{V}^2 \rangle_H$. Many models can be formulated as projected hyperbolic models, starting with the incompressible Euler model. Both the KdV-BBM equations [28, 4] and the Camassa-Holm equations [12] can be demonstrated to fit the projected hyperbolic model framework, as well as high-order dispersive models [36]. For greater physical relevance, while maintaining a reasonable level of complexity, this work will focus on models with the hyperbolic structure of the shallow water equations extended with some tracers, i.e.,

$$H = \begin{pmatrix} h \\ D \end{pmatrix} \quad \text{and} \quad U = \begin{pmatrix} \bar{u} \\ \bar{w}_1 \\ \bar{w}_2 \end{pmatrix}.$$

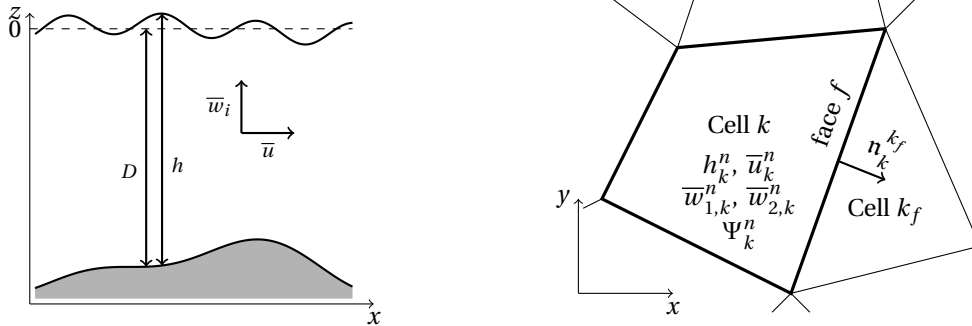


Figure 1: Illustration of the notations: (left) Interpretation of the unknowns in the vertical plan. (right) Finit volume discretization in the horizontal plan.

where $h(t, x) \in \mathbb{R}_+$ represents the water depth, $D(x) \in \mathbb{R}$ denotes the bottom depth, and $\bar{u}(t, x) \in \mathbb{R}^d$ corresponds to the horizontal velocity (refer to Figure 1). The bottom depth D can be treated as an unknown, although it satisfies a trivial equation. The tracers $\bar{w}_1 \in \mathbb{R}$ and $\bar{w}_2 \in \mathbb{R}$ can be interpreted as degrees of freedom of the vertical velocity. Additional details can be found in [17].

Two hyperbolic operators will be considered, where the tracers are either advected with the flow A_{AD} or are steady A_{ST} , namely

$$(6) \quad A_{AD}(H, U) = \begin{pmatrix} \bar{u} & 0 & h & 0 & 0 \\ 0 & 0 & 0 & 0 & 0 \\ g & -g & \bar{u} & 0 & 0 \\ 0 & 0 & 0 & \bar{u} & 0 \\ 0 & 0 & 0 & 0 & \bar{u} \end{pmatrix} \quad \text{and} \quad A_{ST}(H, U) = \begin{pmatrix} \bar{u} & 0 & h & 0 & 0 \\ 0 & 0 & 0 & 0 & 0 \\ g & -g & \bar{u} & 0 & 0 \\ 0 & 0 & 0 & 0 & 0 \\ 0 & 0 & 0 & 0 & 0 \end{pmatrix}.$$

The matrices are not strictly hyperbolic due to multiple eigenvalues involving \bar{u} and 0. However, these multiple eigenvalues are associated with linearly degenerate fields.

Additionally, it is worth noting that for both matrices A_{AD} and A_{ST} , the model (1) can be expressed in a conservative form with a source term. Specifically, defining

$$F_{AD}(W) = \begin{pmatrix} w_2 \\ 0 \\ \frac{w_2^2}{w_0} + \frac{g}{2} w_0^2 \\ \frac{w_2 w_3}{w_0} \\ \frac{w_0 w_4}{w_0} \\ w_0 \end{pmatrix} \quad \text{with} \quad W_{AD} = \mathcal{W}_{AD}(H, U) = \begin{pmatrix} w_0 \\ w_1 \\ w_2 \\ w_3 \\ w_4 \end{pmatrix} = \begin{pmatrix} h \\ D \\ h\bar{u} \\ h\bar{w}_1 \\ h\bar{w}_2 \end{pmatrix}$$

and

$$F_{\text{ST}}(W) = \begin{pmatrix} w_2 \\ 0 \\ \frac{w_2^2}{w_0} + \frac{g}{2} w_0^2 \\ 0 \\ 0 \end{pmatrix} \quad \text{with} \quad W_{\text{ST}} = \mathcal{W}_{\text{ST}}(H, U) = \begin{pmatrix} w_0 \\ w_1 \\ w_2 \\ w_3 \\ w_4 \end{pmatrix} = \begin{pmatrix} h \\ D \\ h\bar{u} \\ D\bar{w}_1 \\ D\bar{w}_2 \end{pmatrix}$$

the projected hyperbolic model (1) with the matrices A_{XX} ($\text{XX} \in \{\text{AD}, \text{ST}\}$) can be written as

$$(7) \quad \partial_t W_{\text{XX}} + \nabla \cdot F_{\text{XX}}(W_{\text{XX}}) = S_{\text{XX}}(W) - h\underline{\Psi}$$

where $S_{\text{ST}}(W) = S_{\text{AD}}(W) = (0, 0, gw_0\nabla w_1, 0, 0)^T$ and $\underline{\Psi} = (0)_{0 \leq i < \text{Dim}(H)}, \Psi)^T$. It is well known that the couple entropy-flux defined by $E(H, U) = \mathcal{P}(H) + \mathcal{K}(H, U)$ with

$$(8) \quad \mathcal{P}(H) = gh\left(\frac{h}{2} - D\right) \quad \text{and} \quad \mathcal{K}(H, U) = \frac{v(H)}{2} U \cdot U \quad \text{with} \quad v(H) = h$$

and the fluxes with and without advection of the tracers respectively reads

$$G_{\text{AD}}(H, U) = G_{\text{ST}}(H, U) + \frac{h\bar{u}}{2} \sum_{i=1}^2 \bar{w}_i^2 \quad \text{and} \quad G_{\text{ST}}(H, U) = \left(g(h - D) + \frac{\bar{u}^2}{2} \right) h\bar{u}$$

satisfies the condition (4).

Obviously, the change of variables $(H, U) \mapsto W$ need to be reversible and in the current cases it reads

$$H = \mathcal{H}_{\text{AD}}(W) = \begin{pmatrix} w_0 \\ w_1 \end{pmatrix} \quad \text{and} \quad U = \mathcal{U}_{\text{AD}}(W) = \begin{pmatrix} \frac{w_2}{w_0} \\ \frac{w_3}{w_0} \\ \frac{w_4}{w_0} \end{pmatrix} \quad \text{if } w_0 > 0, \text{ else } \mathcal{U}_{\text{AD}}(W_{\text{AD}}) = 0$$

or

$$H = \mathcal{H}_{\text{ST}}(W) = \begin{pmatrix} w_0 \\ w_1 \end{pmatrix} \quad \text{and} \quad U = \mathcal{U}_{\text{ST}}(W) = \begin{pmatrix} \frac{w_2}{w_1} \\ \frac{w_3}{w_1} \\ \frac{w_4}{w_1} \end{pmatrix} \quad \text{if } w_1 < 0, \text{ else } \mathcal{U}_{\text{ST}}(W_{\text{ST}}) = 0.$$

2.2.1 Hydrostatic model: the Shallow Water equations

Let us first consider for any $\mathbf{V} = (v_0, v_1, v_2)^T$ the constraint

$$(9) \quad L_H^{\text{SW}}(\mathbf{V}) = \begin{pmatrix} v_1 \\ v_2 \end{pmatrix}.$$

The constraint (9) has no impact on the first velocity variable v_0 and nullifies the other components v_1 and v_2 . It is evident that the projected hyperbolic model (1)

with the hyperbolic operator A_{AD} or A_{ST} defined by (6) and the constraint (9) recovers the classical shallow water equations for any inner product $\langle \mathbf{V}^1, \mathbf{V}^2 \rangle_H$. To clarify, we determine the orthogonal set $\Phi = (\phi_i)_{0 \leq i \leq 2} \in (\mathbb{A}_H^{SW})^\perp$ from $\mathbf{U} = (u_i)_{0 \leq i \leq 2} \in \mathbb{A}_H^{SW}$ by computing the inner product $\langle \mathbf{U}, \Phi \rangle_H$, which vanishes for any u_0 if and only if $\phi_0 = 0$. Consequently, the first two equations of (1) with the hyperbolic operators A_{AD} or A_{ST} and the constraint (9) correspond to the shallow water equations, i.e.

$$(PH^{SW}) \quad \begin{aligned} \partial_t h + \nabla \cdot (h\bar{u}) &= 0 \\ \partial_t \bar{u} + \bar{u} \cdot \nabla \bar{u} &= -g\nabla(h - D). \end{aligned}$$

The constraint (9) is not the sole constraint leading to the shallow water equations (PH^{SW}). Others may be interested in the constraint $L_H^\phi(\mathbf{V}) = \phi$ instead, implying that the projection step has no effect also on the tracers u_1 and u_2 .

2.2.2 Weakly dispersive fully nonlinear models

Now we consider the constraint $L_H^{\text{FN}}(\mathbf{V}) = L[h](\mathbf{V})$ and the inner product $\langle \mathbf{V}^1, \mathbf{V}^2 \rangle_H^{\text{FN}} = P[h](\mathbf{V}^1, \mathbf{V}^2)$ defined by

$$(10) \quad \begin{aligned} L[\mathbf{h}](\mathbf{V}) &= \begin{pmatrix} v_1 + \frac{\mathbf{h}}{2} \nabla \cdot v_0 + v_0 \cdot \nabla D \\ v_2 + \frac{\mathbf{h}}{2\sqrt{3}} \nabla \cdot v_0 \end{pmatrix} \\ \text{and } P[\mathbf{h}](\mathbf{V}^1, \mathbf{V}^2) &= \int_{\mathbb{R}} \mathbf{h} (v_0^1 \cdot v_0^2 + v_1^1 v_1^2 + v_2^1 v_2^2) dx. \end{aligned}$$

As demonstrated in [17], the projected hyperbolic model (1) with the hyperbolic operator A_{AD} defined by (6) and the constraint (10) reproduces the classical Green-Naghdi equations [23]. To clarify, we determine the orthogonal set $\Phi = (\phi_0, \phi_1, \phi_2)^T \in (\mathbb{A}_H^{\text{FN}})^\perp$ from $\mathbf{U} = (u_0, u_1, u_2)^T \in \mathbb{A}_H^{\text{FN}} = \{\mathbf{U} \mid L_H^{\text{FN}}(\mathbf{U}) = 0\}$ by computing

$$\begin{aligned} 0 = \langle \mathbf{U}, \Phi \rangle_H^{\text{FN}} &= \int_{\mathbb{R}^d} h \left(u_0 \cdot \phi_0 - \left(\frac{h}{2} \nabla \cdot u_0 + u_0 \cdot \nabla D \right) \phi_1 - \frac{h}{2\sqrt{3}} \nabla \cdot u_0 \phi_2 \right) dx \\ &= \int_{\mathbb{R}^d} u_0 \cdot \left(h\phi_0 + \nabla \left(\frac{h^2}{2} \left(\phi_1 + \frac{\phi_2}{\sqrt{3}} \right) \right) - h\phi_1 \nabla D \right) dx. \end{aligned}$$

By defining for any $\mathbf{V} \in L_H^2$ the linear operator $R_H^{\text{FN}}(\mathbf{V}) = R[h](\mathbf{V})$ by

$$(11) \quad R[\mathbf{h}](\mathbf{V}) = \mathbf{h}v_0 + \nabla \left(\frac{\mathbf{h}^2}{2} \left(v_1 + \frac{v_2}{\sqrt{3}} \right) \right) - \mathbf{h}v_1 \nabla D$$

we conclude that $(\mathbb{A}_H^{\text{FN}})^\perp = \text{Ker}(R_H^{\text{FN}})$. Applying this operator to the equation of the velocity variable U in (1), we get

$$(12) \quad R_H^{\text{FN}}(\partial_t U + A_{UH} \nabla H + A_{UU} \nabla U) = 0$$

where $A_{UH} \in M_{d_U \times d_H}(\mathbb{R})$ and $A_{UU} \in M_{d_U}(\mathbb{R})$ are, respectively, the left lower block and the right lower block of the hyperbolic operator A . Using the constraint (10)

and the hyperbolic operator A_{AD} defined in (6), the Green-Naghdi equations (in the form [29, (5.11)]) are recovered, i.e.

$$(PH_{\text{AD}}^{\text{FN}}) \quad \begin{aligned} \partial_t h + \nabla \cdot (h\bar{u}) &= 0 \\ (1 + T[h]) (\partial_t \bar{u}) + \bar{u} \cdot \nabla \bar{u} &= -g\nabla(h - D) - (Q^{\text{FN}}[h] + Q_{\text{AD}}[h]) (\bar{u}) \end{aligned}$$

where the dispersive operators are defined by

$$(13) \quad \begin{aligned} T[\mathbf{h}](v_0) &= -\frac{1}{\mathbf{h}} \nabla \left(\frac{\mathbf{h}^3}{3} \nabla \cdot v_0 \right) - \frac{1}{\mathbf{h}} \nabla \left(\frac{\mathbf{h}^2}{2} \nabla D \cdot v_0 \right) + \frac{\mathbf{h}}{2} \nabla D \nabla \cdot v_0 + \nabla D \otimes \nabla D v_0 \\ Q^{\text{FN}}[\mathbf{h}](v_0) &= Q_0[\mathbf{h}](v_0 \cdot \nabla \mathbf{h} \nabla \cdot v_0) + Q_1[\mathbf{h}] (|\nabla \cdot v_0|^2) \\ Q_{\text{AD}}[\mathbf{h}](v_0) &= -Q_0[\mathbf{h}](v_0 \cdot \nabla \mathbf{h} \nabla \cdot v_0) - Q_1[\mathbf{h}](v_0 \cdot \nabla (\nabla \cdot v_0)) \\ &\quad - Q_2[\mathbf{h}](v_0 \cdot \nabla (v_0 \cdot \nabla D)) \end{aligned}$$

$$(14) \quad \begin{aligned} \text{with} \quad Q_0[\mathbf{h}](V) &= \frac{1}{\mathbf{h}} \nabla \left(\frac{\mathbf{h}^2}{3} V \right) - \frac{V}{2} \nabla D \\ Q_1[\mathbf{h}](V) &= \frac{1}{\mathbf{h}} \nabla \left(\frac{\mathbf{h}^3}{3} V \right) - \frac{\mathbf{h}}{2} V \nabla D \\ \text{and} \quad Q_2[\mathbf{h}](V) &= \frac{1}{\mathbf{h}} \nabla \left(\frac{\mathbf{h}^2}{2} V \right) - V \nabla D \end{aligned}$$

The operators $T[\mathbf{h}]$, $Q^{\text{FN}}[\mathbf{h}]$, and $Q_{\text{AD}}[\mathbf{h}]$ are defined to emphasize the contribution of tracer advection in the hyperbolic operator A_{AD} . Some may also be interested in the projected hyperbolic model (1) with the hyperbolic operator A_{ST} defined by (6) and the constraint (10). From (12) and using A_{ST} , we obtain the model

$$(PH_{\text{ST}}^{\text{FN}}) \quad \begin{aligned} \partial_t h + \nabla \cdot (h\bar{u}) &= 0 \\ (1 + T[h]) (\partial_t \bar{u}) + \bar{u} \cdot \nabla \bar{u} &= -g\nabla(h - D) - Q^{\text{FN}}[h] (\bar{u}). \end{aligned}$$

This model was first introduced in [45], and we refer to it as the Yamazaki model thereafter.

Corollary 1. *Since the inner product used for the projection uses the measure of the kinetic energy, i.e., $\langle \mathbf{U}, \Phi \rangle_H^{\text{FN}} = \int_{\mathbb{R}^d} v(H) U \cdot U \, dx$, we conclude using Proposition 1 that the models $(PH_{\text{AD}}^{\text{FN}})$ and $(PH_{\text{ST}}^{\text{FN}})$ conserve the energy E defined in (8). More precisely, one can show that the local energy balance (5) holds with $\mathcal{G} = \mathcal{G}_{\text{ST}}^{\text{FN}}$ for $(PH_{\text{ST}}^{\text{FN}})$ and $\mathcal{G} = \mathcal{G}_{\text{AD}}^{\text{FN}}$ for $(PH_{\text{AD}}^{\text{FN}})$, which reads*

$$\mathcal{G}_{\text{XX}}^{\text{FN}}(H, U) = G_{\text{XX}}(H, U) + \frac{h^2 \bar{u}}{2} \left(\psi_1 + \frac{\psi_2}{\sqrt{3}} \right).$$

Some may interpret the last term of the flow as the vertical integral of the hydrodynamic pressure, see [17].

2.2.3 Weakly dispersive weakly nonlinear models

While linear for the velocity variable, the subspace $(\mathbb{A}_H^{\text{FN}})^\perp$ depends on the time dependent water depth h . From a numerical point of view, this implies that the matrix

of the linear system has to be recomputed at each iteration, significantly slowing down calculations. A classical simplification of fully nonlinear models involves replacing the water depth $h(t, x)$ in the dispersive terms with the bottom depth $D(x)$ under the assumption that the perturbation of the free surface is small enough, i.e. $h = D + O(\varepsilon)$, where ε is the nonlinearity parameter, as seen in [29]. In our framework, this simplification must be applied to the constraint $L_H^{\text{WN}}(\mathbf{V}) = L[D](\mathbf{V})$ and the inner product $\langle \mathbf{V}^1, \mathbf{V}^2 \rangle_H^{\text{WN}} = P[D](\mathbf{V}^1, \mathbf{V}^2)$ defined in (10). Through similar computations to those in §2.2.2, the projected hyperbolic model (1) with the hyperbolic operator A_{ST} and the constraint L_H^{WN} recovers the Peregrine equations [41]. More precisely, the orthogonal set reads $(\mathbb{A}_H^{\text{WN}})^\perp = \text{Ker}(R_H^{\text{WN}})$ with $R_H^{\text{WN}}(\mathbf{V}) = R[D](\mathbf{V})$. Applying this operator to the equation of the velocity variable U in (1), using the constraint L_H^{WN} and the hyperbolic operator A_{ST} , the Peregrine equations (in the form [29, (5.23)]) are recovered, i.e.

$$(PH_{\text{ST}}^{\text{WN}}) \quad \begin{aligned} \partial_t h + \nabla \cdot (h\bar{u}) &= 0 \\ (1 + T[D])(\partial_t \bar{u}) + \bar{u} \cdot \nabla \bar{u} &= -g\nabla(h - D) \end{aligned}$$

with the dispersive operator defined in (13).

Some may also be interested in the projected hyperbolic model (1) with hyperbolic operator A_{AD} and the constraint L_H^{WN} . Applying the operator R_H^{WN} to the equation of the velocity variable U in (1), using the constraint L_H^{WN} and the hyperbolic operator A_{AD} , we obtain the Boussinesq-type model

$$(PH_{\text{AD}}^{\text{WN}}) \quad \begin{aligned} \partial_t h + \nabla \cdot (h\bar{u}) &= 0 \\ (1 + T[D])(\partial_t \bar{u}) + \bar{u} \cdot \nabla \bar{u} &= -g\nabla(h - D) - Q_{\text{AD}}[D](\bar{u}) \end{aligned}$$

A similar model was first introduced in [31].

One consequence of the simplification of the weakly nonlinear model is that the inner product $\langle \mathbf{V}^1, \mathbf{V}^2 \rangle_H^{\text{WN}} \neq \int_{\mathbb{R}^d} v(H) \mathbf{V}_1 \cdot \mathbf{V}_2 \, dx$, hence the Proposition 1 does not hold. Indeed, it is well-known that the weakly dispersive models $(PH_{\text{ST}}^{\text{WN}})$ and $(PH_{\text{AD}}^{\text{WN}})$ do not conserve the energy E as defined in (8).

2.3 Unified projected hyperbolic models

2.3.1 Overview of the general strategy

Let us now explore the space-adaptive modeling of projected hyperbolic models, driven by the considerations outlined in §1. For simplicity, we focus on the coupling of two models: one represented by $PH_{Y_0}^{X_0}$ in a subdomain $\Omega_0 \subset \mathbb{R}^d$ and the other by $PH_{Y_1}^{X_1}$ in a different subdomain $\Omega_1 \subset \mathbb{R}^d$ with $\Omega_0 \cap \Omega_1 = \emptyset$. Our proposed strategy involves formulating a unified projected hyperbolic model and employing a standard resolution method, as detailed in §3.1. Let us introduce the color function $\theta(t, x) \in [0, 1]$, which acts as a parameter for a model denoted as $PH_{Y_1 \theta Y_0}^{X_1 \theta X_0}$ such that $PH_{Y_1 \theta Y_0}^{X_1 \theta X_0}$ recover the model $PH_{Y_0}^{X_0}$ when $\theta = 0$ and $PH_{Y_1}^{X_1}$ when $\theta = 1$. In the point of view of hyperbolic equations, the color function serves as a parameter akin to bathymetry, defining extended variables as $H = (h, D, \theta)^T$ and $U = (\bar{u}, \bar{w}_1, \bar{w}_2)^T$.

As it was done in §2.2 for classical model of the literature, the unified projected hyperbolic model is defined by its hyperbolic operator and its constraint. Note that the coupling of M projected hyperbolic models can be achieved by considering the color function as a vector of $[0, 1]^{M-1}$, and proceed similarly.

The coupling of nonlinear hyperbolic models is extensively addressed in the literature. While specific cases may pose open questions, the coupling of many models, particularly conservative ones, has well-established solutions. For intricate cases, the series of articles [7, 8, 9, 10] provides in-depth discussions. Regarding the relatively simple hyperbolic operators considered in this work, relevant references include [21, 22].

A straightforward coupling strategy involves constructing a unified hyperbolic operator as a linear combination of the hyperbolic operators of the two models being coupled. The advantage of this approach is that if the two models satisfy an entropy relation with the same energy and different fluxes, the unified hyperbolic operators will satisfy an entropy relation by linearity. However, this strategy does not necessarily yield a conservative form (7), and the non-conservative products are typically unclear. Moreover, numerical schemes for approximating solutions of non-conservative hyperbolic models tend to be more complex. Several dispersive models of waves does not satisfy a conservation of energy, such as the Peregrine equations (PH_{ST}^{WN}) or the Yamazaki equations (PH_{ST}^{FN}), so unified models derived from them cannot satisfy it either.

A second coupling strategy, which we will adopt later, was introduced in [22] with the aim of preserving the conservation of variables when both hyperbolic operators exhibit this property. This strategy is based on the continuity of fluxes. The coupled projected hyperbolic model is formulated in the conservative form (7) with the unified conserved variable given by $W_{Y1\varrho_{Y0}} = \theta W_{Y1} + (1 - \theta) W_{Y0}$ and the unified flux $F_{Y1\varrho_{Y0}} = \theta F_{Y1} + (1 - \theta) F_{Y0}$, introducing an additional equation for the evolution for θ . The evolution of θ is not crucial, as its value in practice is fixed by a source-term relaxation operator.

In the case of the coupling of the hyperbolic operator defined in (6), it reads

$$(15) \quad \begin{matrix} W_{AD\varrho_{ST}} \\ \mathcal{W}_{AD\varrho_{ST}}(H, U) \end{matrix} = \begin{pmatrix} w_0 \\ w_1 \\ w_2 \\ w_3 \\ w_4 \\ w_5 \end{pmatrix} = \begin{pmatrix} h \\ D \\ \theta \\ h\bar{u} \\ \hat{h}\bar{w}_1 \\ \hat{h}\bar{w}_2 \end{pmatrix} \quad \text{and} \quad F_{AD\varrho_{ST}}(W) = \begin{pmatrix} w_3 \\ 0 \\ 0 \\ \frac{w_3^2}{2} + \frac{g}{2} w_0^2 \\ \frac{w_0 w_2 w_3 w_4}{2} \\ \frac{\hat{w} w_2 w_3 w_5}{\hat{w}} \end{pmatrix}$$

with $\hat{h} = (\theta h + (1 - \theta) D)$ and $\hat{w} = (w_2 w_0 + (1 - w_2) w_1)$ and the source term $S_{AD\varrho_{ST}}(W) = \left(0, 0, \frac{\bar{\theta} - \theta}{\tau}, g h \nabla D, 0, 0\right)^T$ with $\bar{\theta}(t, x, H)$ is a given function defining where the interface should be and τ is a relaxation time. In practice, τ is assumed small enough such that θ can be confused with $\bar{\theta}$, see §3.1.1.

It is evident that $W_{Y1\varrho_{Y0}}, F_{Y1\varrho_{Y0}}$ tend to W_{Y0} and F_{Y0} when and where $\theta = 0$, and to W_{Y1} and F_{Y1} when and where $\theta = 1$. Then, we can compute the non-conservative form of the unified model (1) with the extended variables H and U . The hyperbolic

operator reads

$$A_{\text{AD}^\theta\text{ST}} = \begin{pmatrix} \bar{u} & 0 & 0 & h & 0 & 0 \\ 0 & 0 & 0 & 0 & 0 & 0 \\ 0 & 0 & 0 & 0 & 0 & 0 \\ g & -g & 0 & \bar{u} & 0 & 0 \\ 0 & 0 & \frac{h\bar{u}\bar{w}_1}{\hat{h}} & 0 & \frac{\theta h\bar{u}}{\hat{h}} & 0 \\ 0 & 0 & \frac{h\bar{u}\bar{w}_2}{\hat{h}} & 0 & 0 & \frac{\theta h\bar{u}}{\hat{h}} \end{pmatrix}.$$

We can easily verify that the matrix $A_{\text{AD}^\theta\text{ST}}$ is hyperbolic. More precisely, its eigenvalues are $\bar{u} \pm \sqrt{g\hat{h}}$ (for the shallow water variables h and \bar{u}), 0 D and θ) and $\frac{\theta h\bar{u}}{\hat{h}}$ (twice for \bar{w}_1 and \bar{w}_2). The change of variables $W \mapsto (H, U)$ reads

$$\mathcal{H}_{\text{AD}^\theta\text{ST}}(W) = \begin{pmatrix} w_0 \\ w_1 \\ w_2 \end{pmatrix} \quad \text{and} \quad \mathcal{U}_{\text{AD}^\theta\text{ST}}(W) = \begin{pmatrix} \frac{w_3}{\hat{w}} \\ \frac{w_4}{\hat{w}} \\ \frac{w_4}{\hat{w}} \end{pmatrix} \quad \text{if } \hat{w} > 0, \text{ else } \mathcal{U}_{\text{AD}^\theta\text{ST}}(W) = 0.$$

Note that the hyperbolic operator $A_{\text{AD}^\theta\text{ST}}$ does not satisfy the entropy relation (4)

In a similar manner, we introduce the constraint in the entire domain

$$(16) \quad \begin{aligned} L_H^{x1^\theta x0}(\mathbf{V}) &= \theta L_H^{x1}(\mathbf{V}) + (1-\theta) L_H^{x0}(\mathbf{V}) \\ \text{and} \quad \langle \mathbf{V}^1, \mathbf{V}^2 \rangle_H^{x1^\theta x0} &= \theta \langle \mathbf{V}^1, \mathbf{V}^2 \rangle_H^{x1} + (1-\theta) \langle \mathbf{V}^1, \mathbf{V}^2 \rangle_H^{x0}. \end{aligned}$$

Note that $L_H^{x1^\theta x0} = L^{x0}$ and $\langle \mathbf{V}^1, \mathbf{V}^2 \rangle_H^{x1^\theta x0} = \langle \mathbf{V}^1, \mathbf{V}^2 \rangle_H^{x0}$ when and where $\theta = 0$, and $L_H^{x1^\theta x0} = L^{x1}$ and $\langle \mathbf{V}^1, \mathbf{V}^2 \rangle_H^{x1^\theta x0} = \langle \mathbf{V}^1, \mathbf{V}^2 \rangle_H^{x1}$ when and where $\theta = 1$.

Finally the coupling of two projected hyperbolic models PH_{Y0}^{x0} and the model PH_{Y1}^{x1} is realized by the unified projected hyperbolic models $PH_{Y1^\theta Y0}^{x1^\theta x0}$ defined using the hyperbolic operator $A_{Y1^\theta Y0}$, the constraint $L_H^{x1^\theta x0}$ and the inner product $\langle \mathbf{V}^1, \mathbf{V}^2 \rangle_H^{x1^\theta x0}$.

2.3.2 Application to fully non-linear and weakly non-linear unified model

The coupling ($PH_{\text{AD}^\theta\text{ST}}^{\text{FN}^\theta\text{WN}}$) between a fully non-linear model ($PH_{\text{AD}}^{\text{FN}}$) and a weakly non-linear model ($PH_{\text{ST}}^{\text{WN}}$) is realized with the help of the constraint defined by (16), which in the present case becomes $L_H^{\text{FN}^\theta\text{WN}}(\mathbf{V}) = L[\hat{h}](\mathbf{V})$ and the inner product $\langle \mathbf{V}^1, \mathbf{V}^2 \rangle_H^{\text{FN}^\theta\text{WN}} = P[\hat{h}](\mathbf{V}^1, \mathbf{V}^2)$ as defined in (10). We remember that $\hat{h} = \theta h + (1-\theta)D$. The orthogonal set $(\mathbb{A}_H^{\text{FN}^\theta\text{WN}})^\perp = \text{Ker}(R_H^{\text{FN}^\theta\text{WN}})$ with $R_H^{\text{FN}^\theta\text{WN}}(\mathbf{V}) = R[\hat{h}](\mathbf{V})$ as defined by (11). Applying this operator to the equation of the velocity variable U in (1), using the constraint $L_H^{\text{FN}^\theta\text{WN}}$ and the hyperbolic operator $A_{\text{AD}^\theta\text{ST}}$, we obtain the unified model

$$(PH_{\text{AD}^\theta\text{ST}}^{\text{FN}^\theta\text{WN}}) \quad \begin{aligned} \partial_t h + \nabla \cdot (h\bar{u}) &= 0 \\ (1 + T[\hat{h}])(\partial_t \bar{u}) + \bar{u} \cdot \nabla \bar{u} &= -g \nabla (h - D) \\ &\quad - \left(Q^{\text{FN}^\theta\text{WN}}[\hat{h}, \theta] + Q_{\text{AD}}^{\text{FN}^\theta\text{WN}}[\hat{h}, \theta] \right) (\bar{u}) \end{aligned}$$

with the operators

$$\begin{aligned} Q^{\text{FN}\ell\text{WN}}[\hat{h}, \theta](v_0) &= Q_0[\hat{h}](\theta v_0 \cdot \nabla h \nabla \cdot v_0) + Q_1[\hat{h}]\left(\frac{\theta h}{\hat{h}} |\nabla \cdot v_0|^2\right) \\ Q_{\text{AD}}^{\text{FN}\ell\text{WN}}[\hat{h}, \theta](v_0) &= -Q_0[\hat{h}]\left(\frac{h}{\hat{h}} v_0 \cdot \nabla (\theta \hat{h}) \nabla \cdot v_0\right) - Q_1[\hat{h}]\left(\frac{\theta h}{\hat{h}} v_0 \cdot \nabla (\nabla \cdot v_0)\right) \\ &\quad - Q_2[\hat{h}]\left(\frac{h}{\hat{h}} v_0 \cdot \nabla (\theta v_0 \cdot \nabla D)\right) \end{aligned}$$

where $Q_0[\mathbf{h}]$, $Q_1[\mathbf{h}]$ and $Q_2[\mathbf{h}]$ are defined in (14).

The coupling $(PH_{\text{ST}}^{\text{FN}\ell\text{WN}})$ between the Yamazaki model $(PH_{\text{ST}}^{\text{FN}})$ and the Peregrine model $(PH_{\text{ST}}^{\text{WN}})$ can be realized in a similar way with the hyperbolic operator A_{ST} . We obtain the coupled model

$$\begin{aligned} (PH_{\text{ST}}^{\text{FN}\ell\text{WN}}) \quad \partial_t h + \nabla \cdot (h \bar{u}) &= 0 \\ (1 + T[\hat{h}])(\partial_t \bar{u}) + \bar{u} \cdot \nabla \bar{u} &= -g \nabla (h - D) - Q^{\text{FN}\ell\text{WN}}[\hat{h}, \theta](\bar{u}) \end{aligned}$$

The coupling $(PH_{\text{AD}}^{\text{FN}\ell\text{WN}})$ between the Green-Naghdi model $(PH_{\text{AD}}^{\text{FN}})$ and the Boussinesq-type model $(PH_{\text{AD}}^{\text{WN}})$ is realized in a similar way using the hyperbolic operator A_{AD} . We obtain the coupled model

$$\begin{aligned} (PH_{\text{AD}}^{\text{FN}\ell\text{WN}}) \quad \partial_t h + \nabla \cdot (h \bar{u}) &= 0 \\ (1 + T[\hat{h}])(\partial_t \bar{u}) + \bar{u} \cdot \nabla \bar{u} &= -g \nabla (h - D) \\ &\quad - \left(Q^{\text{FN}\ell\text{WN}}[\hat{h}, \theta] + Q_{\text{AD}}[\hat{h}] \right) (\bar{u}) \end{aligned}$$

As with the classical weakly non-linear models, the coupled models $(PH_{\text{AD}\text{ST}}^{\text{FN}\ell\text{WN}})$ $(PH_{\text{ST}}^{\text{FN}\ell\text{WN}})$ and $(PH_{\text{AD}}^{\text{FN}\ell\text{WN}})$ do not conserve the energy E in the form defined in (8), since the inner product of the projection is not defined thanks to the kinetic energy of the hyperbolic operator and thus the Proposition 1 cannot be applied.

2.3.3 Application to fully non-linear and hydrostatic models

The coupling $(PH_{\text{AD}}^{\text{FN}\ell\text{SW}})$ between the Green-Naghdi model $(PH_{\text{AD}}^{\text{FN}})$ and the hydrostatic shallow water model (PH^{SW}) is realized using the constraint defined by (16), which in the present case becomes $L_H^{\text{FN}\ell\text{SW}}(\mathbf{V}) = L_\theta[h](\mathbf{V})$ with

$$(17) \quad L_\theta[\mathbf{h}](\mathbf{V}) = \begin{pmatrix} v_1 + \theta \left(\frac{\mathbf{h}}{2} \nabla \cdot v_0 + v_0 \cdot \nabla D \right) \\ v_2 + \theta \left(\frac{\mathbf{h}}{2\sqrt{3}} \nabla \cdot v_0 \right) \end{pmatrix}$$

and the inner product $\langle \mathbf{V}^1, \mathbf{V}^2 \rangle_H^{\text{FN}\ell\text{SW}} = \langle \mathbf{V}^1, \mathbf{V}^2 \rangle_H^{\text{FN}} = P[h](\mathbf{V}^1, \mathbf{V}^2)$ defined in (10). By performing the same calculations as in §2.2.2, we obtain that the orthogonal set $(\mathbb{A}_H^{\text{FN}\ell\text{SW}})^\perp = \text{Ker}(R_H^{\text{FN}\ell\text{SW}})$ with $R_H^{\text{FN}\ell\text{SW}}(\mathbf{V}) = R_\theta[h](\mathbf{V})$ is defined as

$$(18) \quad R_\theta[\mathbf{h}](\mathbf{V}) = \mathbf{h} v_0 + \nabla \left(\frac{\theta \mathbf{h}^2}{2} \left(v_1 + \frac{v_2}{\sqrt{3}} \right) \right) - \theta \mathbf{h} v_1 \nabla D.$$

Finally, if we apply this operator to the equation of the velocity variable U in (1), use the constraint $L_H^{\text{FN}^\theta\text{SW}}$ and the hyperbolic operator A_{AD} , we obtain the coupled model

$$(PH_{\text{AD}}^{\text{FN}^\theta\text{SW}}) \quad \begin{aligned} \partial_t h + \nabla \cdot (h\bar{u}) &= 0 \\ (1 + T_\theta[h]) (\partial_t \bar{u}) + \bar{u} \cdot \nabla \bar{u} &= -g \nabla (h - D) \\ &\quad - \left(Q^{\text{FN}^\theta\text{SW}}[h, \theta] + Q_{\text{AD}}^{\text{FN}^\theta\text{SW}}[h, \theta] \right) (\bar{u}) \end{aligned}$$

with the operators

$$(19) \quad \begin{aligned} T_\theta[\mathbf{h}](v_0) &= -\frac{1}{\mathbf{h}} \nabla \left(\frac{\theta^2 \mathbf{h}^3}{3} \nabla \cdot v_0 \right) - \frac{1}{\mathbf{h}} \nabla \left(\frac{\theta^2 \mathbf{h}^2}{2} \nabla D \cdot v_0 \right) \\ &\quad + \frac{\theta^2 \mathbf{h}}{2} \nabla D \nabla \cdot v_0 + \theta^2 \nabla D \otimes \nabla D v_0 \\ Q^{\text{FN}^\theta\text{SW}}[\mathbf{h}, \theta](v_0) &= Q_0[\mathbf{h}] (\theta^2 v_0 \cdot \nabla \mathbf{h} \nabla \cdot v_0) + Q_1[\mathbf{h}] (\theta^2 |\nabla \cdot v_0|^2) \\ Q_{\text{AD}}^{\text{FN}^\theta\text{SW}}[\mathbf{h}, \theta](v_0) &= -Q_0[\mathbf{h}] (\theta v_0 \cdot \nabla (\theta \mathbf{h}) \nabla \cdot v_0) - Q_1[\mathbf{h}] (\theta^2 v_0 \cdot \nabla (\nabla \cdot v_0)) \\ &\quad - Q_2[\mathbf{h}] (\theta v_0 \cdot \nabla (\theta v_0 \cdot \nabla D)) \end{aligned}$$

where $Q_0[\mathbf{h}]$, $Q_1[\mathbf{h}]$ and $Q_2[\mathbf{h}]$ are defined in (14).

The coupling ($PH_{\text{ST}}^{\text{FN}^\theta\text{SW}}$) between a Yamazaki model ($PH_{\text{ST}}^{\text{FN}}$) and the hydrostatic shallow water model (PH^{SW}) is realized in a similar way using the hyperbolic operator A_{ST} . We obtain the coupled model

$$(PH_{\text{ST}}^{\text{FN}^\theta\text{SW}}) \quad \begin{aligned} \partial_t h + \nabla \cdot (h\bar{u}) &= 0 \\ (1 + T_\theta[h]) (\partial_t \bar{u}) + \bar{u} \cdot \nabla \bar{u} &= -g \nabla (h - D) - Q^{\text{FN}^\theta\text{SW}}[h, \theta] (\bar{u}) \end{aligned}$$

Corollary 2. *Since the inner product used for the projection uses the measure of the kinetic energy, i.e. $\langle \mathbf{U}, \Phi \rangle_H^{\text{FN}} = \int_{\mathbb{R}^d} v(H) U \cdot U \, dx$, using Proposition 1, we conclude that the models ($PH_{\text{AD}}^{\text{FN}^\theta\text{SW}}$) and ($PH_{\text{ST}}^{\text{FN}^\theta\text{SW}}$) conserve the energy E defined in (8). More precisely, it can be shown that the local energy balance (5) hold with $\text{xx} \in \{\text{AD}, \text{ST}\}$ and $\mathcal{G} = \mathcal{G}_{\text{xx}}^{\text{FN}^\theta\text{SW}}$ applies to $PH_{\text{xx}}^{\text{WN}^\theta\text{SW}}$, which is*

$$\mathcal{G}_{\text{xx}}^{\text{FN}^\theta\text{SW}}(H, U) = G_{\text{xx}}(H, U) + \theta \frac{h^2 \bar{u}}{2} \left(\psi_1 + \frac{\psi_2}{\sqrt{3}} \right).$$

2.3.4 Application to weakly non-linear and hydrostatic models

The coupling ($PH_{\text{ST}}^{\text{WN}^\theta\text{SW}}$) between the Peregrine model ($PH_{\text{ST}}^{\text{WN}}$) and the hydrostatic shallow water model (PH^{SW}) is realized using the constraint defined by (16), which in the present case becomes $L_H^{\text{FN}^\theta\text{SW}}(\mathbf{V}) = L_\theta[D](\mathbf{V})$, defined in (17) and the inner product $\langle \mathbf{V}^1, \mathbf{V}^2 \rangle_H^{\text{WN}^\theta\text{SW}} = \langle \mathbf{V}^1, \mathbf{V}^2 \rangle_H^{\text{WN}} = P[D](\mathbf{V}^1, \mathbf{V}^2)$, defined in (10). The orthogonal set $\left(\mathbb{A}_H^{\text{WN}^\theta\text{SW}} \right)^\perp = \text{Ker} \left(R_H^{\text{WN}^\theta\text{SW}} \right)$ with $R_H^{\text{WN}^\theta\text{SW}}(\mathbf{V}) = R_\theta[D](\mathbf{V})$, defined by (18). Applying this operator to the equation of the velocity variable U in (1), using the constraint $L_H^{\text{WN}^\theta\text{SW}}$ and the hyperbolic operator A_{ST} , we obtain the coupled model

$$(PH_{\text{ST}}^{\text{WN}^\theta\text{SW}}) \quad \begin{aligned} \partial_t h + \nabla \cdot (h\bar{u}) &= 0 \\ (1 + T_\theta[D]) (\partial_t \bar{u}) + \bar{u} \cdot \nabla \bar{u} &= -g \nabla (h - D) \end{aligned}$$

with the operator $T_\theta[D]$ defined in (19).

The coupling $(PH_{AD}^{WN\theta-sw})$ between a Boussinesq-type model (PH_{AD}^{WN}) and the hydrostatic shallow water model (PH^{sw}) is realized in a similar way with the hyperbolic operator A_{AD} . We obtain the coupled model

$$(PH_{AD}^{WN\theta-sw}) \quad \begin{aligned} \partial_t h + \nabla \cdot (h\bar{u}) &= 0 \\ (1 + T_\theta[D]) (\partial_t \bar{u}) + \bar{u} \cdot \nabla \bar{u} &= -g\nabla(h - D) - Q_{AD}^{FN\theta-sw}[D, \theta](\bar{u}) \end{aligned}$$

with the operators defined in (19).

As with the classical weakly nonlinear models, the coupled models $(PH_{ST}^{WN\theta-sw})$ and $(PH_{AD}^{WN\theta-sw})$ do not conserve the energy E as defined in (8), since the inner product of the projection is not defined thanks to the kinetic energy of the hyperbolic operator and therefore the Proposition 1 cannot be applied.

3 Discrete framework

The current section is devoted to the numerical resolution of a general projected hyperbolic model. This resolution is based on a splitting between the hyperbolic operator and the dispersive source term. This splitting is often used for the numerical resolution of dispersive models, see [1, 13, 15, 16, 31, 35, 38, 42]. In the current work, we follow the numerical strategy proposed in [40] because it is based on the projection relation (3) that we used for the coupling, also because it ensures entropy stability at the discrete level, i.e. a discrete counterpart of (5) and stability for a family of boundary conditions see [39]. Note that the projection relation is not essential for the numerical resolution of the (1) model, not even for the unified models $PH_{y1\theta y0}^{x1\theta x0}$. The strategies mentioned above can probably be used.

3.1 Overview of the numerical scheme

We consider a tessellation \mathbb{T} of the horizontal domain $\Omega \subset \mathbb{R}^d$ consisting of $\text{Card}(\mathbb{T})$ star-shaped control volumes, see Figure 1. We denote by $k \in \mathbb{T}$ a control volume on the tessellation, by \mathbb{F}_k the set of its faces and by m_k its surface area. In addition, for a face f , its length is denoted by m_f and the neighbor of k by f is denoted by k_f , e.g. $k \cup k_f = f$. The unit normal to f outwards to k is denoted by $\mathbf{n}_k^{k_f}$. We consider a finite volume scheme, so that the numerical unknowns ϕ_k^n for $\phi \in \{h, \bar{u}, \bar{w}_1, \bar{w}_2, \Psi\}$ and the vectorial notations H , U and W are the averaged values in the control volume k at time t^n of the physical unknowns ϕ .

The first parts of the section are devoted to the description of a numerical scheme for a general projected hyperbolic model. §3.1.1 describes a Godunov-type scheme for the hyperbolic operator, while §3.1.2 describes the correction step that uses the projection relation (3). Note that the hyperbolic operator can be discretized with any kind of method, in particular explicit schemes are not required. This strategy was already used in [40] for the Green-Naghdi equations. We describe the projection scheme for the coupling of dispersive models in §3.2 and for the coupling with the shallow water equations in §3.3.

3.1.1 Hyperbolic step

The first step of the numerical scheme is the resolution of the hyperbolic operator. In order to use the most classical hyperbolic schemes, we assume in this paper that the hyperbolic operator can be written under the conservative form (7). We propose to use an explicit conservative Godunov-type scheme, i.e. we set

$$(20) \quad W_k^{n*} = W_k^n - \frac{\delta_t^n}{m_k} \sum_{f \in \mathbb{F}_k} \mathcal{F}_f^n \cdot \mathbf{n}_k^{k_f} m_f - \delta_t^n \mathcal{S}_k^n$$

where $t^n = t^{n-1} + \delta_t^n$, \mathcal{F}_f^n is a numerical approximation of the flux $\mathcal{F}_{\text{YY}}(W)$ at time t^n and through the face f and \mathcal{S}_k^n is a numerical approximation of the source term $S_{\text{YY}}(W)$ at time t^n and on the control volume k . In practice, the real unknowns of this step are the unknowns of the shallow water plus the two tracers $h, \bar{u}, \bar{w}_1, \bar{w}_2$, since the fluxes of the depth D and the color θ vanish.

Several strategies for computing the numerical flux \mathcal{F}_f^n and the source term \mathcal{S}_k^n of the shallow water equations are described in the literature, see [6, 20, 34, 43]. The Godunov-type schemes are stable under a CFL condition of the form

$$(21) \quad \lambda(W_k^n; W_{k_f}^n) \delta_t^n \leq \min(\delta_k, \delta_{k_f})$$

with δ_k the compactness of k_f , i.e. $\delta_k = \frac{m_k}{2}$ if $d = 1$ and $\delta_k = \frac{m_k}{\sum_{f \in \mathbb{F}_k} m_f}$ if $d = 2$. $\lambda(W_L; W_R)$ is an upper limit of the wave speed, depending on the numerical flux \mathcal{F} used, see [6]. In practice, we use an HLL scheme in this work to compute the water depth h_k^n and the horizontal velocity normal to the face $\bar{u}_k^n \cdot \mathbf{n}_k^{k_f}$ and an upwind scheme (using the mass flux) for the horizontal velocity parallel to the face $\bar{u}_k^n \cdot (\mathbf{n}_k^{k_f})^\perp$ and the tracers \bar{w}_1 and \bar{w}_2 . The bathymetry source term is treated with the hydrostatic reconstruction [3]. The relaxation time of the color θ is also assumed to be small enough so that it can be approximated by the given function at each time step, i.e.

$$\theta_k^n = \bar{\theta}(t^n, x_k, H_k^n).$$

At the end of this step, we compute the potential variables $H_k^{n+1} = \mathcal{H}_{\text{YY}}(W_k^{n+1})$ and the velocity variable $U_k^{n+1} = \mathcal{U}_{\text{YY}}(W_k^{n+1})$ from the conservative variable W_k^{n+1} . For a variable ϕ that is discretized on the tessellation, we find that $\phi_\star = (\phi_k)_{k \in \mathbb{T}}$ and the product term to term means $u_\star \phi_\star = (u_k \phi_k)_{k \in \mathbb{T}}$.

3.1.2 Projection step

Since the dispersive source term for the potential variable disappears, we first set $H_\star^{n+1} = H_\star^{n*}$. As a continuous description, the numerical scheme then only requires the discretization $L_{H_\star}(\mathbf{V}_\star)$ of the constraint $L_H(U)$ and $\langle \mathbf{V}_\star^1, \mathbf{V}_\star^2 \rangle_{H_\star}$ of the inner product $\langle \mathbf{V}^1, \mathbf{V}^2 \rangle_H$ respectively. From this, we calculate the discrete counterpart Ψ_\star of the dispersion source term Ψ , which ensures orthogonality with every element that fulfills the constraint. The boundary conditions act at this level. Assuming that the orthogonal relation continues to hold on a bounded domain, a

condition appears at the boundary of the domain, see [39] for the Green-Naghdi model. In the present work, we will not consider the boundary condition for the sake of simplicity and consider, for example, a periodic spatial domain. Then for any $\mathbf{U}_\star \in \mathbb{A}_{H_\star} = \{\mathbf{U}_\star \mid L_{H_\star}(\mathbf{U}_\star) = 0\}$ we determine \mathbb{A}_{H_\star} , so that for any $\Phi_\star \in \mathbb{A}_{H_\star}^\perp$ we have

$$(22) \quad \langle \mathbf{U}_\star, \Phi_\star \rangle_{H_\star} = 0$$

which leads to the relation $R_{H_\star}(\Phi_\star) = 0$. Finally, the projection step consists of decomposing the discrete functions \mathbf{U}_\star into the subspace $\mathbb{A}_{H_\star^{n+1}}$ and $\mathbb{A}_{H_\star^{n+1}}^\perp$ which leads to the solution of the linear system with the unknowns U_\star^{n+1} and Ψ_\star^{n+1}

$$(23) \quad \begin{aligned} U_\star^{n+1} &= U_\star^{n*} - \delta_t^n \Psi_\star^{n+1} \\ L_{H_\star^{n+1}}(U_\star^{n+1}) &= 0 \\ R_{H_\star^{n+1}}(\Psi_\star^{n+1}) &= 0. \end{aligned}$$

To highlight a stability result that generalizes the stability results [40, Proposition 4 and 7], we introduce the discrete linear space $L_{H_\star}^2 := \{\mathbf{V}_\star \mid \langle \mathbf{V}_\star, \mathbf{V}_\star \rangle_{H_\star} < \infty\}$.

Proposition 2. *Assume that the hyperbolic scheme (20) is entropy-satisfying, i.e.*

$$\sum_{k \in \mathbb{T}} E(H_k^{n*}, U_k^{n*}) \mathfrak{m}_k \leq \sum_{k \in \mathbb{T}} E(H_k^n, U_k^n) \mathfrak{m}_k$$

and the discrete inner product is defined by

$$\langle \mathbf{V}_\star^1, \mathbf{V}_\star^2 \rangle_{H_\star} = \sum_k v(H_k) \mathbf{V}_k^1 \cdot \mathbf{V}_k^2 \mathfrak{m}_k$$

where $v(H)$ is associated to the kinetic energy. Then for any initial data with finite energy, i.e. $\sum_{k \in \mathbb{T}} E(H_k^0, U_k^0) \mathfrak{m}_k < \infty$, the linear system (23) is well-posed and the global scheme is entropy-satisfying, i.e.

$$\sum_{k \in \mathbb{T}} E(H_k^{n+1}, U_k^{n+1}) \mathfrak{m}_k \leq \sum_{k \in \mathbb{T}} E(H_k^n, U_k^n) \mathfrak{m}_k.$$

Proof. Thank to the orthogonality relation (22), we have $L_{H_\star}^2 = \mathbb{A}_{H_\star} \oplus \mathbb{A}_{H_\star}^\perp$, so that the linear system (23) is well posed for any $U_\star^{n*} \in L_{H_\star}^2$.

Also using the Pythagorean theorem, we have

$$\langle U_\star^{n*}, U_\star^{n*} \rangle_{H_\star^{n+1}} = \langle U_\star^{n+1}, U_\star^{n+1} \rangle_{H_\star^{n+1}} + |\delta_t^n|^2 \langle \Psi_\star^{n+1}, \Psi_\star^{n+1} \rangle_{H_\star^{n+1}}$$

hence we conclude that $\sum_k \mathcal{K}(H_k^{n+1}, U_k^{n+1}) \mathfrak{m}_k \leq \sum_k \mathcal{K}(H_k^{n+1}, U_k^{n*}) \mathfrak{m}_k$. Since the potential variable is not affected by the second step of the scheme we have

$$\sum_{k \in \mathbb{T}} E(H_k^{n+1}, U_k^{n+1}) \mathfrak{m}_k \leq \sum_{k \in \mathbb{T}} E(H_k^{n*}, U_k^{n*}) \mathfrak{m}_k$$

and we conclude since the hyperbolic scheme is assumed entropy-satisfying. \square

The linear system (23) can be solved by a smaller linear system using the constraint L_{H_\star} and R_{H_\star} . For example, if we apply $R_{H_\star^{n+1}}$ to the first equation of (23), we get $R_{H_\star^{n+1}}(U_\star^{n+1}) = R_{H_\star^{n+1}}(U_\star^{n*})$, then the dispersive source term can be explicitly derived by $\Psi_\star^{n+1} = \frac{U_\star^{n*} - U_\star^{n+1}}{\delta_t^n}$. Or vice versa, if we apply $L_{H_\star^{n+1}}$ to the first equation of (23), we get $\delta_t^n L_{H_\star}(\Psi_\star^{n+1}) = L_{H_\star}(U_\star^{n*})$ then $U_\star^{n+1} = U_\star^{n*} - \delta_t^n \Psi_\star^{n+1}$. In practice, the system can be reduced even further to a linear system of size $\min\left(\text{Dim}\left(\mathbb{A}_{H_\star^{n+1}}\right), \text{Dim}\left(\mathbb{A}_{H_\star^{n+1}}^\perp\right)\right)$ see further (25). At the end of this step, we compute the conservative variables $W_k^{n+1} = \mathcal{W}_{YY}(H_k^{n+1}, U_k^{n+1})$ from the variables for the potential H_k^{n+1} and the velocity U_k^{n+1} . As it is the scheme is globally first order. However, it was shown in [40] that following the strategy proposed in [24], a high order scheme can be proposed with only one implicate projection step.

3.2 Application to fully non-linear and weakly non-linear unified model

In this section, the projection step for the coupling of weakly nonlinear and fully nonlinear dispersive models is described in detail. We propose to use the simple discretization of the constraints $L_{H_\star, \star}^{\text{FN}}(\mathbf{V}_\star) = L_\star^c[h_\star](\mathbf{V}_\star)$ and $L_{H_\star, \star}^{\text{WN}}(\mathbf{V}_\star) = L_\star^c[D_\star](\mathbf{V}_\star)$ so $L_{H_\star, \star}^{\text{FN} \oplus \text{WN}}(\mathbf{V}_\star) = L_\star^c[h_{\theta, \star}](\mathbf{V}_\star)$ with $h_{\theta, k} = \theta_k h_k + (1 - \theta_k) D_k$ and

$$(24) \quad L_k^c[\mathbf{h}_\star](\mathbf{V}_\star) = \begin{pmatrix} v_{1,k} + \frac{\mathbf{h}_k}{2} \nabla_k^c \cdot v_{0,\star} + v_{0,k} \cdot \nabla_k^c D_\star \\ v_{2,k} + \frac{\mathbf{h}_k}{2\sqrt{3}} \nabla_k^c \cdot v_{0,\star} \end{pmatrix}$$

where the centered approximation is used to discretize the divergence and the gradient, i.e.

$$\nabla_k^c \cdot \phi_\star = \frac{1}{m_k} \sum_{\mathbb{F}_k} \frac{\phi_k + \phi_{k_f}}{2} \cdot \mathbf{n}_k^{k_f} m_f \quad \text{and} \quad \nabla_k^c \phi_\star = \frac{1}{m_k} \sum_{\mathbb{F}_k} \frac{\phi_k + \phi_{k_f}}{2} \mathbf{n}_k^{k_f} m_f.$$

We will also use the discrete inner products $\langle \mathbf{V}_\star^1, \mathbf{V}_\star^2 \rangle_{H_\star}^{\text{FN}} = P^c[h_\star](\mathbf{V}_\star^1, \mathbf{V}_\star^2)$ and $\langle \mathbf{V}_\star^1, \mathbf{V}_\star^2 \rangle_{H_\star}^{\text{WN}} = P^c[D_\star](\mathbf{V}_\star^1, \mathbf{V}_\star^2)$ so $\langle \mathbf{V}_\star^1, \mathbf{V}_\star^2 \rangle_{H_\star}^{\text{FN} \oplus \text{WN}} = P^c[h_{\theta, \star}](\mathbf{V}_\star^1, \mathbf{V}_\star^2)$ with

$$P^c[\mathbf{h}_\star](\mathbf{V}_\star^1, \mathbf{V}_\star^2) = \sum_{k \in \mathbb{T}} \mathbf{h}_k \mathbf{V}_k^1 \cdot \mathbf{V}_k^2 m_k.$$

Then we determine the orthogonal set $\left(\mathbb{A}_{H_\star}^{\text{XX}}\right)^\perp$ of $\mathbb{A}_{H_\star}^{\text{XX}} = \left\{ \mathbf{U}_\star \mid L_{H_\star, k}^{\text{XX}}(\mathbf{U}_\star) = 0 \right\}$. As in the continuous case, the boundary conditions act on this plane and lead to an additional relation at the boundary that must be satisfied to ensure the projection, see [39]. In the present work, we assume a periodic boundary for simplification. In the periodic domain, the following relation applies

$$\sum_{k \in \mathbb{T}} a_k \cdot \nabla_k^c b_\star m_k = \sum_{k \in \mathbb{T}} b_\star \nabla_k^c \cdot a_\star m_k.$$

Hence for any $\mathbf{U}_\star \in \mathbb{A}_{H_\star}^{\text{XX}}$ and any $\Phi_\star \in \left(\mathbb{A}_{H_\star}^{\text{XX}}\right)^\perp$, we have

$$\begin{aligned} 0 &= P^c[\mathbf{h}_\star](\mathbf{U}_\star, \Phi_\star) = \sum_{k \in \mathbb{T}} \mathbf{h}_k (u_{0,k} \cdot \phi_{0,k} + u_{1,k} \cdot \phi_{1,k} + u_{2,k} \cdot \phi_{2,k}) \mathbf{m}_k \\ &= \sum_{k \in \mathbb{T}} \mathbf{h}_k \left(u_{0,k} \cdot \phi_{0,k} - \frac{\mathbf{h}_k}{2} \left(\phi_{1,k} + \frac{\phi_{2,k}}{\sqrt{3}} \right) \nabla_k^c \cdot u_{0,\star} - u_{0,k} \cdot \phi_{1,k} \nabla_k^c D_\star \right) \mathbf{m}_k \\ &= \sum_{k \in \mathbb{T}} u_{0,k} \cdot \left(\mathbf{h}_k \phi_{0,k} + \nabla_k^c \left(\frac{\mathbf{h}_k^2}{2} \left(\phi_{1,\star} + \frac{\phi_{2,\star}}{\sqrt{3}} \right) \right) - \mathbf{h}_k \phi_{1,k} \nabla_k^c D_\star \right) \mathbf{m}_k \end{aligned}$$

We conclude that $\left(\mathbb{A}_{H_\star}^{\text{XX}}\right)^\perp = \text{Ker}\left(R_{H_\star, \star}^{\text{XX}}\right)$ with $R_{H_\star, \star}^{\text{FN}} = R_\star^c[h_\star]$, $R_{H_\star, \star}^{\text{WN}} = R_\star^c[D_\star]$ and $R_{H_\star, \star}^{\text{FN}^\theta\text{WN}} = R_\star^c[\hat{h}_{0,\star}]$ with the discrete counterpart of the operator (11)

$$R_k^c[\mathbf{h}_\star](V_\star) = \mathbf{h}_k v_{0,k} + \nabla_k^c \left(\frac{\mathbf{h}_k^2}{2} \left(v_{1,\star} + \frac{v_{2,\star}}{\sqrt{3}} \right) \right) - \mathbf{h}_k v_{1,k} \nabla_k^c D_\star.$$

Applying $R_{H_\star, \star}^{\text{XX}}$ to the first equations of the projection scheme (23) we obtain $R_\star^c[\mathbf{h}_\star^{n+1}](U_\star^{n+1}) = R_\star^c[\mathbf{h}_\star^{n+1}](U_\star^{n*})$ and using the constraint $L_\star^c[\mathbf{h}_\star](U_\star^{n+1}) = 0$ the linear system (23) finally resume to the elliptic equation of the horizontal velocity

$$(25) \quad \alpha_k^{\text{XX}} \bar{u}_k^{n+1} - \mu_k^{\text{XX}} \nabla_k^c \cdot \bar{u}_\star^{n+1} + \nabla_k^c (\mu_k^{\text{XX}} \cdot \bar{u}_\star^{n+1}) - \nabla_k^c (\kappa_k^{\text{XX}} \nabla_\star \cdot \bar{u}_\star^{n+1}) = \beta_k^{\text{XX}}$$

with

- $\alpha_k^{\text{FN}} = \alpha_k[h_\star^{n+1}]$, $\mu_k^{\text{FN}} = \mu_k[h_\star^{n+1}]$, $\kappa_k^{\text{FN}} = \kappa_k[h_\star^{n+1}]$ and $\beta_k^{\text{FN}} = \beta_k[h_\star^{n+1}]$;
- $\alpha_k^{\text{WN}} = \alpha_k[D_\star^{n+1}]$, $\mu_k^{\text{WN}} = \mu_k[D_\star^{n+1}]$, $\kappa_k^{\text{WN}} = \kappa_k[D_\star^{n+1}]$ and $\beta_k^{\text{WN}} = \beta_k[D_\star^{n+1}]$;
- $\alpha_k^{\text{FN}^\theta\text{WN}} = \alpha_k[\hat{h}_\star^{n+1}]$, $\mu_k^{\text{FN}^\theta\text{WN}} = \mu_k[\hat{h}_\star^{n+1}]$, $\kappa_k^{\text{FN}^\theta\text{WN}} = \kappa_k[\hat{h}_\star^{n+1}]$ and $\beta_k^{\text{FN}^\theta\text{WN}} = \beta_k[\hat{h}_\star^{n+1}]$;

$$\begin{aligned} \text{with} \quad \alpha_k[\mathbf{h}_\star] &= \mathbf{h}_k + \mathbf{h}_k \nabla_k^c D_\star \otimes \nabla_k^c D_\star, \quad \mu_k[\mathbf{h}_\star] = -\frac{|\mathbf{h}_k|^2}{2} \nabla_k^c D_\star \\ \kappa_k[\mathbf{h}_\star] &= \frac{|\mathbf{h}_k|^3}{3} \quad \text{and} \quad \beta_k[\mathbf{h}_\star] = R^c[\mathbf{h}_\star](U_\star^{n*}). \end{aligned}$$

The projection step can be summarized by solving the linear system (25) to compute \bar{u}_\star^{n+1} , then $\bar{w}_{1,\star}^{n+1}$ and $\bar{w}_{2,\star}^{n+1}$ are explicitly computed such that $L_k^c[\mathbf{h}_\star^{n+1}](U_\star^{n+1}) = 0$, i.e. setting

$$\bar{w}_{1,k} = -\frac{\mathbf{h}_k}{2} \nabla_k^c \cdot \bar{u}_\star - \bar{u}_k \cdot \nabla_k^c D_\star \quad \text{and} \quad \bar{w}_{2,k} = -\frac{\mathbf{h}_k}{2\sqrt{3}} \nabla_k^c \cdot \bar{u}_\star.$$

3.3 Application to weakly dispersive and hydrostatic unified model

In this section, the projection step for the coupling of shallow water equations with weakly dispersive models is described in detail. We propose the discretization of the constraints $L_{H_\star, \star}^{\text{FN}}(\mathbf{V}_\star) = L_\star^c[h_\star](\mathbf{V}_\star)$ and $L_{H_\star, \star}^{\text{WN}}(\mathbf{V}_\star) = L_\star^c[D_\star](\mathbf{V}_\star)$ as defined in (24).

The constraint of the shallow water equations is simply $L_{H_\star, k}^{\text{SW}}(\mathbf{V}_\star) = (v_{1,k}, v_{2,k})^T$. The constraint of the coupling is therefore

$$(26) \quad L_{H_\star, k}^{\text{X1}^\ell\text{SW}}(\mathbf{V}_\star) = \begin{pmatrix} v_{1,k} + \theta \left(\frac{\mathbf{h}_k}{2} \nabla_k^c \cdot v_{0,\star} + v_{0,k} \cdot \nabla_k^c D_\star \right) \\ v_{2,k} + \theta \left(\frac{\mathbf{h}_k}{2\sqrt{3}} \nabla_k^c \cdot v_{0,\star} \right) \end{pmatrix}$$

with $\mathbf{h}_\star = h_\star$ if $\text{X1} = \text{FN}$ and $\mathbf{h}_\star = D_\star$ if $\text{X1} = \text{WN}$. Since the shallow water equations do not depend on the inner product used for the projection, we use the dispersive model $\langle \mathbf{V}_\star^1, \mathbf{V}_\star^2 \rangle_{H_\star}^{\text{FN}}$ or $\langle \mathbf{V}_\star^1, \mathbf{V}_\star^2 \rangle_{H_\star}^{\text{WN}}$ everywhere.

Then we determine the orthogonal set $\left(\mathbb{A}_{H_\star}^{\text{X1}^\ell\text{SW}} \right)^\perp$ of $\mathbb{A}_{H_\star}^{\text{X1}^\ell\text{SW}} = \{ \mathbf{U}_\star \mid L_{H_\star, k}^{\text{X1}^\ell\text{SW}}(\mathbf{U}_\star) = 0 \}$.

For any $\mathbf{U}_\star \in \mathbb{A}_{H_\star}^{\text{X1}^\ell\text{SW}}$ and any $\Phi_\star \in \left(\mathbb{A}_{H_\star}^{\text{X1}^\ell\text{SW}} \right)^\perp$ we have

$$\begin{aligned} 0 &= P^c[\mathbf{h}_\star](\mathbf{U}_\star, \Phi_\star) = \sum_{k \in \mathbb{T}} \mathbf{h}_k (u_{0,k} \cdot \phi_{0,k} + u_{1,k} \cdot \phi_{1,k} + u_{2,k} \cdot \phi_{2,k}) \mathbf{m}_k \\ &= \sum_{k \in \mathbb{T}} \mathbf{h}_k \left(u_{0,k} \cdot \phi_{0,k} - \frac{\theta_k \mathbf{h}_k}{2} \left(\phi_{1,k} + \frac{\phi_{2,k}}{\sqrt{3}} \right) \nabla_k^c \cdot u_{0,\star} - \theta_k u_{0,k} \cdot \phi_{1,k} \nabla_k^c D_\star \right) \mathbf{m}_k \\ &= \sum_{k \in \mathbb{T}} u_{0,k} \cdot \left(\mathbf{h}_k \phi_{0,k} + \nabla_k^c \left(\frac{\theta_\star \mathbf{h}_\star^2}{2} \left(\phi_{1,\star} + \frac{\phi_{2,\star}}{\sqrt{3}} \right) \right) - \theta_k \mathbf{h}_k \phi_{1,k} \nabla_k^c D_\star \right) \mathbf{m}_k \end{aligned}$$

We conclude that $\left(\mathbb{A}_{H_\star}^{\text{XX}} \right)^\perp = \text{Ker} \left(R_{H_\star}^{\text{X1}^\ell\text{SW}} \right)$ with

$$R_{H_\star, k}^{\text{X1}^\ell\text{SW}}(\mathbf{V}_\star) = \mathbf{h}_k v_{0,k} + \nabla_k^c \left(\frac{\theta_\star \mathbf{h}_\star^2}{2} \left(v_{1,\star} + \frac{v_{2,\star}}{\sqrt{3}} \right) \right) - \theta_k \mathbf{h}_k v_{1,k} \nabla_k^c D_\star.$$

If we apply $R_{H_\star, \star}^{\text{X1}^\ell\text{SW}}$ to the first equations of the projection scheme (23), we obtain $R_{H_\star, \star}^{\text{X1}^\ell\text{SW}}(U_\star^{n+1}) = R_{H_\star, \star}^{\text{X1}^\ell\text{SW}}(U_\star^{n*})$ and using the constraint $L_{H_\star, \star}^{\text{X1}^\ell\text{SW}}(U_\star^{n+1}) = 0$, the linear system (23) finally goes into the elliptic equation (25) with the parameters

$$\begin{aligned} \alpha_k^{\text{X1}^\ell\text{SW}} &= \mathbf{h}_k^{n+1} + \theta_k^2 \mathbf{h}_k^{n+1} \nabla_k^c D_\star \otimes \nabla_k^c D_\star, & \mu_k^{\text{X1}^\ell\text{SW}} &= -\frac{\theta_k^2 |\mathbf{h}_k^{n+1}|^2}{2} \nabla_k^c D_\star \\ \kappa_k^{\text{X1}^\ell\text{SW}} &= \theta_k^2 \frac{|\mathbf{h}_k^{n+1}|^3}{3} & \text{and} & \quad \beta_k^{\text{X1}^\ell\text{SW}} = R_{H_\star, k}^{\text{X1}^\ell\text{SW}}(U_\star^{n*}). \end{aligned}$$

The projection step can be summarized by solving the linear system (25) to compute \bar{u}_\star^{n+1} , then $\bar{w}_{1,\star}^{n+1}$ and $\bar{w}_{2,\star}^{n+1}$ are explicitly computed such that $L_k^c[\mathbf{h}_\star](U_\star) = 0$, i.e. setting

$$v_{1,k} = -\theta \left(\frac{\mathbf{h}_k}{2} \nabla_k^c \cdot v_{0,\star} + v_{0,k} \cdot \nabla_k^c D_\star \right) \quad \text{and} \quad v_{2,k} = -\theta \frac{\mathbf{h}_k}{2\sqrt{3}} \nabla_k^c \cdot v_{0,\star}.$$

Note that the numerical scheme coupling the Green-Naghdi equations with the shallow water equations $PH_{\text{AD}}^{\text{FN}^\ell\text{SW}}$ is entropy-satisfying since it fulfills the assumptions of Proposition 2.

3.4 Some practical remarks on the numerical scheme

We would like to emphasize the following points for the numerical computation:

- i) The way it is currently presented, the values for the unknowns D and θ are computed in the hyperbolic step but remain unchanged. Obviously in practice, the computations related to these variables are not carried out.
- ii) Where the shallow water equations are under consideration, i.e. when $\theta_k^n = 0$, the linear system (25) simplifies to $\bar{u}_k^{n+1} = \bar{u}_k^{n*}$. Consequently, the solution of the linear system (25) can be confined to the region where $\theta_k^n \neq 0$, resulting in a reduction of computation time.
- iii) An advantage of employing the weakly nonlinear models (PH_{ST}^{WN}) or (PH_{AD}^{WN}) is that the matrix of the linear system (25) remains independent of time. Inverting this matrix (or factoring it) is advantageous once at the simulation's initialization and subsequently apply this inversion to the right-hand side throughout the simulation. This advantage is less apparent in cases involving coupling with fully nonlinear models, as seen in ($PH_{AD}^{FN\theta WN}$), ($PH_{AD}^{FN\theta WN}$), ($PH_{ST}^{FN\theta WN}$), (??). When the color function θ remains constant in the part of the domain where the weakly nonlinear model is applicable, i.e., $\theta_k = 0$, there is no need to estimate the coefficients of the matrix of the linear system (25) at each time step. However, the entire system still needs to be solved at each iteration, akin to the fully nonlinear models. Despite this, it is still feasible to independently solve the weakly nonlinear model portion using an iterative block method, such as the block-Jacobi or block-Gauss-Seidel methods. This strategy proves to be advantageous, especially in the context of domain decomposition for large simulations, where the decomposition aligns with the boundaries of the subdomain where $\theta_k = 0$.

4 Numerical validation

This section is dedicated to illustrating the coupling strategy proposed in the current work through various numerical experiments. We consider a homogeneous 1D tessellation given by $\mathbb{T} = [1, N] \cap \mathbb{N}$, where N is the number of control volumes, and the spatial step is $\delta_x = m_k = \frac{m_\Omega}{N}$, with m_Ω being the domain size. Throughout all simulations, the gravity acceleration g is set to 9.81. Also the color function θ remains constant in time, defined as $\bar{\theta}(x) = \theta^0(x)$. The analysis of time-dependent θ functions, for example, in the context of breaking waves, will be considered in future works.

In Section 4.1, we conduct a thorough parameter analysis of the method in a simple scenario, i.e. a traveling wave on flat bottom passing through the coupling interface. We illustrate then how to take advantage of the method with two typical cases, by imposing time-dependent boundary conditions §4.2 and for the propagation over a discontinuous bottom §4.3.

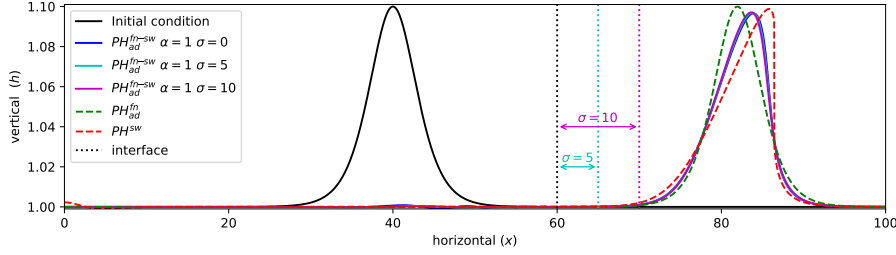


Figure 2: §4.1 – Water depth at time $t = \frac{40}{\sqrt{g\mu m_\Omega}}$ of $(PH_{AD}^{FN\theta_{SW}})$ with some interface thicknesses $\sigma = 0$, $\sigma = 5$ and $\sigma = 10$ with the initial condition (27) with $\mu = 10^{-2}$, $\varepsilon = 10^{-1}$ and $\delta_x = 10^{-3}$.

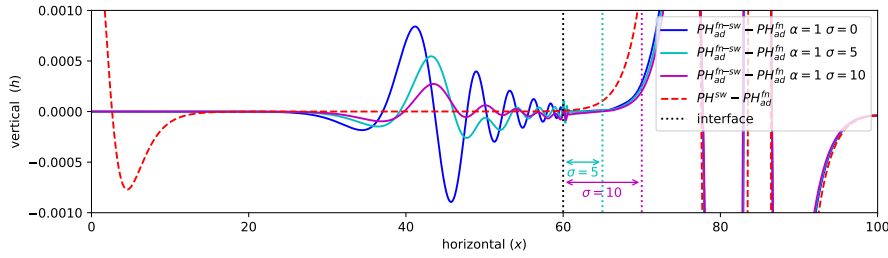


Figure 3: §4.1 – Reflected waves at time $t = \frac{40}{\sqrt{g\mu m_\Omega}}$ of $(PH_{AD}^{FN\theta_{SW}})$ with $\alpha = 1$ and $\sigma = 0$, $\sigma = 5$ and $\sigma = 10$ with the initial condition (27) with $\mu = 10^{-2}$, $\varepsilon = 10^{-1}$ and $\delta_x = 10^{-3}$.

4.1 Coupling between dispersive and hydrostatic models

We consider the following test case: a solitary wave propagating over a flat bottom in a 1D domain with a length of $m_\Omega = 100$. The solitary wave (of the Green-Naghdi equations (PH_{AD}^{FN})) is initially centered at $x^0 = 40$ and travels to the right, i.e.

$$(27) \quad \begin{aligned} h^0(x) &= \mu m_\Omega \left(1 + \varepsilon \left(\operatorname{sech} \left(\sqrt{\frac{0.75\varepsilon}{1+\varepsilon}} \frac{x - x^0}{\mu m_\Omega} \right) \right)^2 \right) \\ \text{and} \quad u^0(x) &= \left(1 - \frac{\mu m_\Omega}{h^0(x)} \right) \sqrt{g\mu m_\Omega (1 + \varepsilon)} \end{aligned}$$

where μ is the shallowness parameter and ε the nonlinearity parameter. The bottom depth $D = \mu m_\Omega$ since the bottom is flat. The color function θ is defined by

$$\theta(x) = \begin{cases} 1 & , \text{ for } x \leq 60 \\ 1 - \left(\frac{x-60}{\sigma} \right)^\alpha & , \text{ for } 60 \leq x \leq 60 + \sigma \\ 0 & , \text{ for } 60 + \sigma \leq x \end{cases}$$

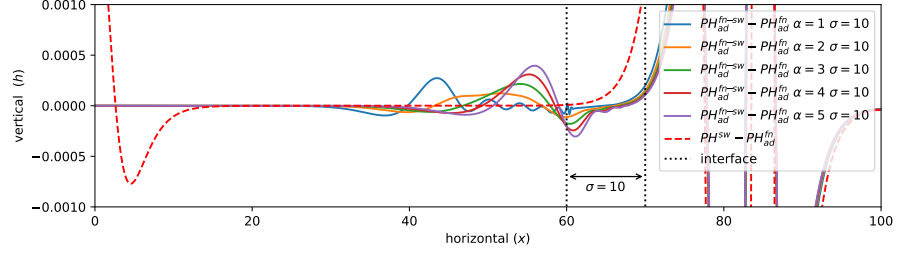


Figure 4: §4.1 – Reflected waves at time $t = \frac{40}{\sqrt{g\mu m\Omega}}$ of $(PH_{AD}^{FN\theta-SW})$ with $\sigma = 10$ and $\alpha \in [1, 5]$ with the initial condition (27) with $\mu = 10^{-2}$, $\varepsilon = 10^{-1}$ and $\delta_x = 10^{-3}$.

where σ is the thickness of the interface and α control the regularity at $x = 60$. If $\sigma = 0$, the interface is sharpe such that $\theta = 1$ for $x < 60$ and $\theta = 0$ for $x > 60$ for any α . The boundary condition are define as wall at both sides, i.e. $u(t, 0) = u(t, m_\Omega) = 0$.

The discrete initial conditions are defined as follows: $h_k^0 = h^0((k-1/2)\delta_x)$, $\bar{u}_k^0 = \bar{u}^0((k-1/2)\delta_x)$ and $\theta_k = \theta((k-1/2)\delta_x)$, where δ_x is the spatial step. The additional velocity variables, $\bar{w}_{1,k}^0$ and $\bar{w}_{2,k}^0$, are determined such that $L_{H^0}(U^0) = 0$. To enforce the discrete wall boundary conditions, a mirror flow approach is employed, i.e. we set $h_0^n = h_1^n$, $\bar{u}_0^n = -\bar{u}_1^n$, $\bar{u}_{-1}^n = -\bar{u}_2^n$, $\bar{w}_{i,0}^n = \bar{w}_{i,1}^n$; $h_{N+1}^n = h_N^n$, $\bar{u}_{N+1}^n = -\bar{u}_N^n$, $\bar{u}_{N+2}^n = -\bar{u}_{N-1}^n$, and $\bar{w}_{i,N+1}^n = \bar{w}_{i,N}^n$.

Let's discuss the results obtained through the coupling of the weakly dispersive model with the shallow water equations. In Figure 2, the water depth obtained with the fully nonlinear weakly dispersive model $(PH_{AD}^{FN\theta-SW})$ is plotted at time $t = \frac{40}{\sqrt{g\mu m\Omega}}$ with $\delta_x = 10^{-3}$, $\mu = 10^{-2}$, $\varepsilon = 10^{-1}$, and various interface thickness values $\sigma = 0$, $\sigma = 5$, and $\sigma = 10$ with $\alpha = 1$. For comparison, the results obtained with the uncoupled Green-Naghdi equations (PH_{AD}^{FN}) using the same projection scheme and the shallow water equations (PH^{SW}) are also plotted. Observations indicate that the wave of the coupled model falls between the waves obtained with the uncoupled models (PH_{AD}^{FN}) and (PH^{SW}) . Additionally, it's noteworthy that the amplitude of the wave in the coupled model is slightly smaller than the waves of the uncoupled models, even though the shallow water equations have not yet developed shocks. This reduction in amplitude is attributed to the reflection of a portion of the wave at the interface.

In Figure Figure 3, the difference between the water depth obtained with the coupled model $(PH_{AD}^{FN\theta-SW})$ and the uncoupled Green-Naghdi equations (PH_{AD}^{FN}) is plotted at time $t = \frac{40}{\sqrt{g\mu m\Omega}}$ with $\delta_x = 10^{-3}$, $\mu = 10^{-2}$, $\varepsilon = 10^{-1}$, and various interface thickness values $\sigma = 0$, $\sigma = 5$, and $\sigma = 10$ with $\alpha = 1$. As anticipated, the amplitude of the reflected waves diminishes with increasing interface thickness. The reflected waves originate at the boundary of the dispersive model, $x = 60$, and subsequently propagate to the left. In Figure 4, the same simulations are conducted with $\sigma = 10$ and varying values of α from 1 to 5. The results demonstrate that the solutions are

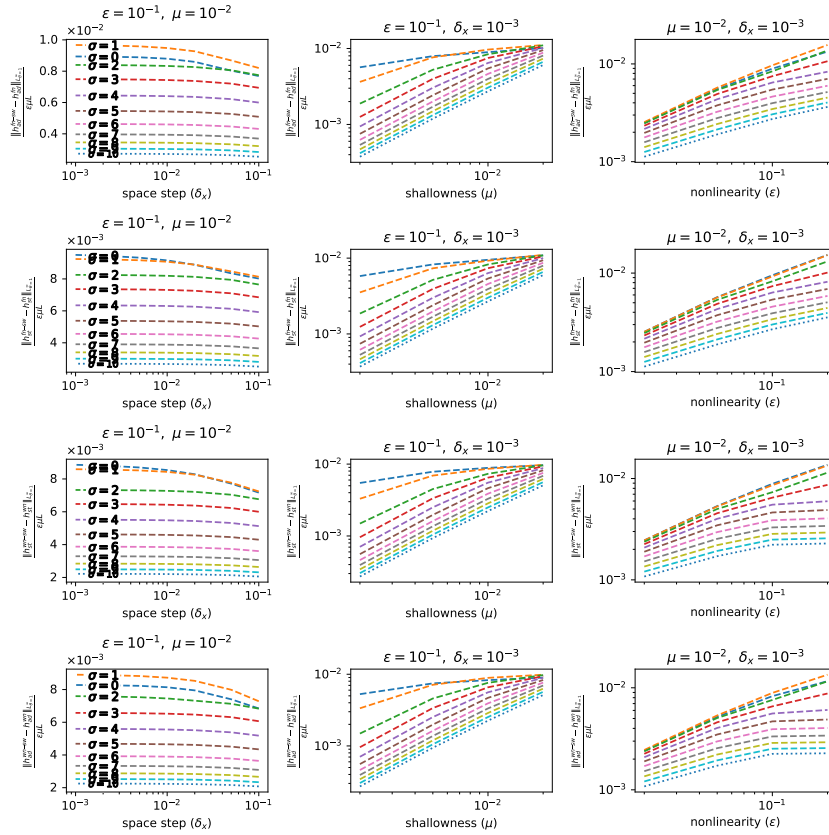


Figure 5: §4.1 – Amplitude of the reflected waves of the models $(PH_{AD}^{FN^{\theta}SW})$ (first line), $(PH_{ST}^{FN^{\theta}SW})$ (second line), $(PH_{ST}^{WN^{\theta}SW})$ (third line) and $(PH_{AD}^{WN^{\theta}SW})$ (fourth line) with $\alpha = 1$ as function of the parameters δ_x (left column), μ (center column) and ϵ (right column).

smoother at $x = 60$, even if the reflected waves have the same amplitude. Optimal results appear to be achieved for $\alpha = 2$, where θ is regular at $x = 60$ but without to large variations in the interface.

In this section, we aim to provide a detailed characterization of the amplitude of the reflected waves. Figure 5 (first line) illustrates the normalized amplitude of the reflected waves generated by the model $(PH_{AD}^{FN^{\theta}SW})$. The plots showcase the dependence on the space step δ_x (left column), the shallowness parameter μ (centered column), and the nonlinearity parameter ϵ (right column). The investigation spans various values of the thickness parameter σ ranging from 0 to 10, with $\alpha = 1$. Notably, all parameters, except those explicitly under study, are set to fixed values: $\delta_x = 10^{-3}$, $\mu = 10^{-2}$, and $\epsilon = 10^{-1}$. The amplitude of the reflected waves is quantified as the difference between the outcomes of the coupled model $(PH_{AD}^{FN^{\theta}SW})$ and the un-

coupled models (PH_{AD}^{FN}) in the region of the domain where $\theta = 1$. This quantification is precisely defined by the norm

$$\left\| h_{YY}^{X0\ell_{sw}} - h_{YY}^{X0} \right\|_{L_{\theta=1}^{\infty}} = \max_{1 \leq N_{out} \leq 100} \max_{1 \leq k \leq \lfloor \frac{60}{\delta_x} \rfloor} \left(\left(h_{YY}^{X0\ell_{sw}} \right)_k^{N_{out}} - \left(h_{YY}^{X0} \right)_k^{N_{out}} \right)$$

with N_{out} is the number of the output such that the solution at iteration N_{out} is an approximation of the solution at time $t = \frac{0.4N_{out}}{\sqrt{g\mu m_{\Omega}}}$. The water depth h_{XX}^{YY} corresponds to the water depth obtained using the numerical scheme for the model PH_{XX}^{YY} . For clarity, the reflected waves have been normalized by the amplitude of the initial condition $\varepsilon\mu m_{\Omega}$.

From the left picture of Figure 5, it becomes apparent that the amplitude of the reflected waves converges as δ_x goes to zero, aligning with the expectation that the numerical scheme for the coupled model ($PH_{AD}^{FN\ell_{sw}}$) is entropy-satisfying. This observation leads us to conclude that the observed wave is not a numerical artifact but rather an inherent property of the coupled model ($PH_{AD}^{FN\ell_{sw}}$), where the color function θ undergoes variations. This behavior can be rationalized by the dynamic nature of the wave celerity in ($PH_{AD}^{FN\ell_{sw}}$), which changes spatially with the color function θ . As the interface thickness σ increases, the color function θ becomes more regular, resulting in a reduction of the amplitude of the reflection waves. However, it's worth noting that the decay of the reflection waves is not particularly rapid, and in practical terms, it remains unclear if increasing the interface thickness is a feasible solution to mitigate this effect. Nevertheless, the amplitude of the reflected wave remains below 1% of the initial wave, even at stiff interfaces.

The center and right pictures of Figure 5 illustrate the dependency of the reflected waves on the physical parameters μ and ε . It is evident that the normalized amplitude of the reflected waves predominantly decreases with both physical parameters, regardless of the interface thickness σ . Specifically, for sufficiently large interface thickness, it appears that the amplitude of the reflected waves can be expressed as

$$\left\| h_{AD}^{FN\ell_{WN}} - h_{AD}^{FN} \right\|_{L_{\theta=1}^{\infty}} \approx O\left(\varepsilon^{\frac{3}{2}}\mu^2\right).$$

In conclusion, we find that the coupling does not introduce an error greater than the modeling error inherent in the shallow water equations, which is of the order μ .

The same results are obtained for the models ($PH_{ST}^{FN\ell_{sw}}$), ($PH_{ST}^{WN\ell_{sw}}$) and ($PH_{AD}^{WN\ell_{sw}}$) as shown respectively on Figure 5 second line, third line and fourth line.

4.2 Application to boundary conditions

In this section, we illustrate how to take advantage of the coupling strategy to impose a temporal signal as a boundary condition. To achieve this, we consider a 1D domain with $m_{\Omega} = 100$, initially at rest with $h^0 = 1$ and $u^0 = 0$, and study the propagation of a plane wave given by

$$(28) \quad \begin{aligned} \tilde{h}(t, x) &= 1 + \varepsilon \cos(\omega t - kx) \\ \tilde{u}(t, x) &= \varepsilon \sqrt{g} \cos(\omega t - kx) \end{aligned}$$

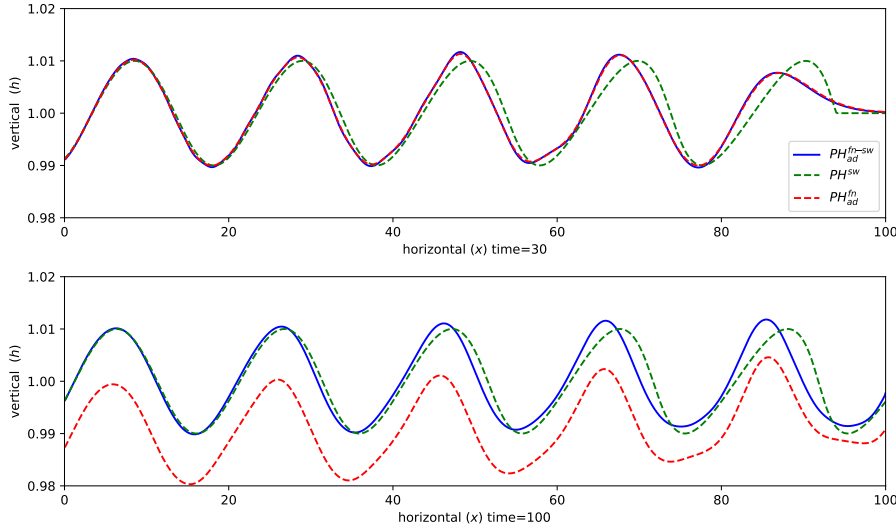


Figure 6: §4.2 – Water depth at time $t = 30$ (first line) and $t = 100$ (second line) obtained with (PH^{SW}) , (PH_{AD}^{FN}) and $(PH_{AD}^{FN\theta-SW})$ with $\varepsilon = 10^{-2}$.

with ω representing the frequency and k denoting the wave number. Due to the non-linearity, the waves (28) are not solutions of the models. Additionally, owing to the dispersion relation of the models, the frequency and wave number are interrelated. For all the models considered above, the dispersion relation is expressed as

$$(29) \quad \omega(k) = \frac{gk}{1 + \frac{|kD|^2}{3}}$$

except for the shallow water equations (PH^{SW}) where $\omega(k) = gk$. To impose the signal at the boundaries, we employ different methods depending on the models:

- For the shallow water equations (PH^{SW}) , we enforce the water depth at the left boundary of the domain, $h(t, 0) = \tilde{h}(t, 0)$. At the discrete level, this is achieved by setting $h_0^n = \tilde{h}(t^n, 0)$, and the velocity is computed to preserve the outward Riemann invariant: $\bar{u}_0^n = \bar{u}_1^n + 2\left(\sqrt{gh_0^n} - \sqrt{gh_1^n}\right)$ see [20]. To maintain the constraint $L_H^{SW}(U)$ at the boundaries, we set $\bar{w}^n|_{i=0} = 0$. For the right boundary, a transparent (free) boundary condition can be imposed by considering homogeneous Neumann boundary conditions for all the unknowns. At the discrete level, this involves setting $h_{N+1}^n = h_N^n$, $\bar{u}_{N+1}^n = \bar{u}_N^n$, and $\bar{w}_{i,N+1}^n = \bar{w}_{i,N}^n$.
- For the dispersive models (PH_{AD}^{FN}) , (PH_{ST}^{FN}) , (PH_{ST}^{WN}) , or (PH_{AD}^{WN}) , we enforce the discharge and the hydrodynamic pressure at the left boundary of the domain as proposed in [39, §5.2]. This strategy involves fixing the discharge at the boundary, the hydrodynamic pressure, and the vertical velocities. In this document, the hydrodynamic pressure at the boundary is neglected, and the

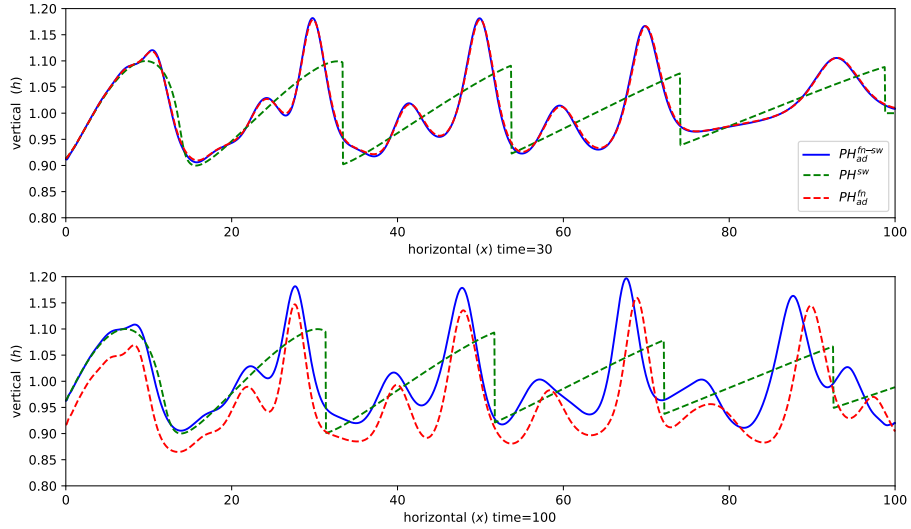


Figure 7: §4.2 – Water depth at time $t = 30$ (first line) and $t = 100$ (second line) obtained with (PH^{sw}) , (PH_{AD}^{fn}) and $(PH_{AD}^{fn\theta-sw})$ with $\varepsilon = 10^{-1}$.

vertical velocity \bar{w}_1^n is computed using the constraint $L_H^{xx}(U)$ of the model. For the right boundary, we use the transparent boundary condition as proposed in [39, §5.1.2].

- One application of the coupled models $(PH_{AD}^{fn\theta-sw})$, $(PH_{ST}^{fn\theta-sw})$, $(PH_{ST}^{wn\theta-sw})$ or $(PH_{AD}^{wn\theta-sw})$ is to impose boundary conditions similar to those for the shallow water equations (PH^{sw}) by setting $\theta = 0$ close to the boundaries. In practice, we set $\theta_k = 0$ only for the two control volumes closest to each bound, i.e., $k \in \{1, 2, N-1, N\}$, and $\theta_k = 1$ in the rest of the domain. The thickness of the shallow water domain corresponds to the stencil of the linear system (25). It is noteworthy that certain boundary conditions of the dispersive models cannot be specified using this technique, especially those involving non-vanishing hydrodynamic pressure at the boundary. However, for many practical cases, specifying time series of water depths at the boundaries suffices, and this aligns with the current scenario.

The results of simulations have been plotted in Figure 6 with $\delta_x = 10^{-2}$, the wave number $k = 10^{-1}$, the frequency ω computed with (29) (even for (PH^{sw})), and $\varepsilon = 10^{-2}$. On the first line, we display the results at time 30, before the wave reaches the right boundary. It is observed that the results obtained with (PH_{AD}^{fn}) and $(PH_{AD}^{fn\theta-sw})$ are nearly identical, validating the boundary condition on the right. The main advantage of imposing the boundary condition with the coupled model lies in its simplicity. On the second line, the results at time 100 are plotted, after several periods have left the domain. Due to a small wave reflected at the right boundary, the results

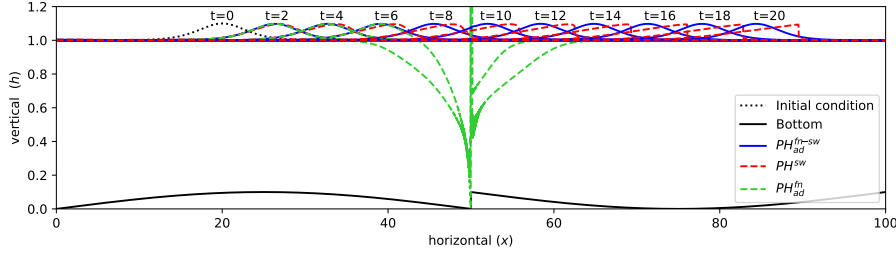


Figure 8: §4.3 – Water depth obtained with (PH^{SW}) (red lines), (PH_{AD}^{FN}) (green lines) and $(PH_{AD}^{FN\theta-SW})$ (bleu lines) with $b = 10^{-1}$.

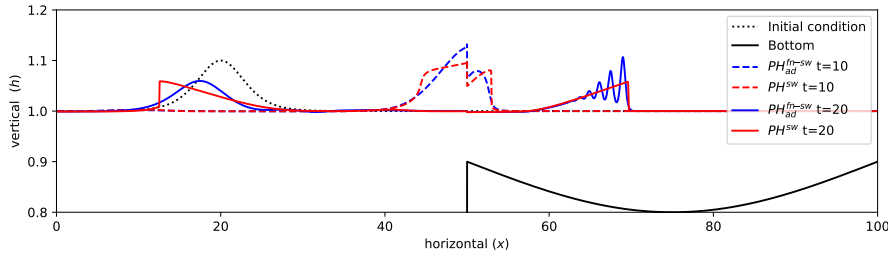


Figure 9: §4.3 – Water depth obtained with (PH^{SW}) (red lines) and $(PH_{AD}^{FN\theta-SW})$ (bleu lines) with $b = 9 \cdot 10^{-1}$ at time $t=10$ (dashed lines) and $t=20$ (solid lines).

of (PH_{AD}^{FN}) are shifted, and the mean water depth is not correct, as it is not fixed by the left boundary condition. A better transparent boundary condition for the Green-Naghdi equations could potentially correct this drawback (see [25]). With the coupled model $(PH_{AD}^{FN\theta-SW})$, the reflection at the right boundary almost disappears, and the mean water depth is fixed at the left boundary condition regardless. Higher non linear waves can be simulated as well, as shown in Figure 7, where the simulations were plotted with the same parameters except for ε , which was set to 10^{-1} . Similar results were observed with the other models $(PH_{ST}^{FN\theta-SW})$, $(PH_{ST}^{WN\theta-SW})$, or $(PH_{AD}^{WN\theta-SW})$.

4.3 Application to discontinuous bathymetry

In this section, we illustrate how to take advantage of the coupling strategy to simulate the propagation of a wave over a discontinuous bottom. As indicated in [30], dispersive models are only well-posed with a bottom that is slightly more regular than Lipschitz, i.e. $W^{1+s,\infty}$ with $s > 0$. In our framework, this limitation can be understood by the fact that with a non-Lipschitz bottom, the constraint $L[\mathbf{h}](\mathbf{V})$ defined by (10) does not define a linear subspace. However, this is not the case for the constraint $L^{SW}(\mathbf{V})$ defined in (9). It is noteworthy that the shallow water model

is not clearly derived over a discontinuous bottom [18]; it is not well-posed due to non-conservative product [6], and its numerical approximation can lead to different results using different schemes [2]. Nevertheless, many numerical schemes for the shallow water model are stable and used for practical applications. The objective of this section is to propose a stable numerical strategy to perform numerical simulations of dispersive models over a discontinuous bottom.

Let us consider in a 1D domain with $m_\Omega = 100$ with wall boundary conditions and initially a solitary wave given by (27) with $\chi^0 = 20$, $\mu = 10^{-2}$ and $\varepsilon = 10^{-1}$ traveling over a non-flat bottom given by

$$(30) \quad D(x) = -1 + 10^{-1} \sin\left(\frac{2\pi x}{100}\right) + b \mathbb{1}_{[50:100]}$$

with b the amplitude of the discontinuity of bottom. To conduct the simulation with the coupled model ($PH_{AD}^{FN\theta SW}$), we set $\theta = 1 - \mathbb{1}_{[50-2\delta_x:50+2\delta_x]}$. This ensures that the thickness of the domain where $\theta = 0$ is minimized, yet sufficient for the projection step not to encounter the discontinuity of the bottom.

In Figure 8, we show the results obtained with (PH^{SW}) (red lines), (PH_{AD}^{FN}) (green lines) and ($PH_{AD}^{FN\theta SW}$) (bleu lines) with a small discontinuity $b = 10^{-1}$. After time $t = 4$, the results of ($PH_{AD}^{FN\theta SW}$) become significantly not relevant. A discontinuity of the velocity is observed at the discontinuity of the bottom, positive at the left of the discontinuity and negative at the right. This leads to the formation of a hole in the water that grown in time until time $t = 8$ where the water depth vanishes. Note that the simulation of (PH_{AD}^{FN}) with the scheme described in §3 can simulate the propagation of waves over continuous bottom without any problem as shown in [40]. The results obtained with (PH^{SW}) and ($PH_{AD}^{FN\theta SW}$) do not seem inconsistent over the discontinuity. For larger discontinuities of the bottom, we observed that the wave above the discontinuity of the bottom become discontinuous for both (PH^{SW}) and ($PH_{AD}^{FN\theta SW}$), see Figure 9 for $b = 9 \cdot 10^{-1}$. Although probably unphysical, this discontinuity does not interfere with the simulation and the transmitted and reflected waves seem consistent with what we expect. Obviously, the relevance of the numerical results required more comparisons with finer model like 3D Navier-Stokes or observations.

In Figure 8, we present the results obtained with (PH^{SW}) (red lines), (PH_{AD}^{FN}) (green lines), and ($PH_{AD}^{FN\theta SW}$) (blue lines) over a small discontinuity $b = 10^{-1}$. Beyond time $t = 4$, the results of the uncouple model (PH_{AD}^{FN}) become significantly less relevant. A discontinuity in velocity is observed at the bottom's discontinuity, positive to the left and negative to the right. This leads to the formation of a hole in the water, growing over time until it vanishes at $t = 8$ where the water depth becomes zero. It is noteworthy that the simulation of (PH_{AD}^{FN}) with the scheme described in §3 can successfully simulate wave propagation over continuous bottoms, as shown in [40]. The results obtained with (PH^{SW}) and ($PH_{AD}^{FN\theta SW}$) do not appear inconsistent over the discontinuity. For larger bottom discontinuity, we observed that the wave becomes discontinuous for both (PH^{SW}) and ($PH_{AD}^{FN\theta SW}$), as seen in Figure 9 for $b = 9 \cdot 10^{-1}$. Although potentially unphysical, this discontinuity does not disrupt the simulation,

and the transmitted and reflected waves seem consistent with expectations. It is essential to acknowledge that the relevance of numerical results requires further comparison with more refined models, such as 3D Navier-Stokes, or validation through experimental data.

5 Conclusion

In this work, we provide a general overview of the projected hyperbolic models, encompassing several existing dispersive models from the literature. This generalization allows us to extend previous results, including the study of boundary conditions [39] and the development of entropy-satisfying numerical schemes [40], to all models respecting this structure. Additionally, the general framework facilitates the formulation of continuous and discrete couplings of dispersive models while preserving essential properties like energy conservation. We illustrate the usefulness of the method through two applications known to present challenges for dispersive models, namely the imposition of a time signal as a boundary condition, and wave propagation over a discontinuous bottom.

The focus of this work was primarily on classical weakly dispersive models, either coupled together or with a shallow water model. A natural extension of this work would involve high-order dispersive models [36, 37]. Specifically, coupling weakly dispersive models with high-order dispersive models could be explored to optimize computation time by restricting the use of high-order models to regions where they are most needed. Another intriguing extension could involve investigating time-dependent θ functions, such as those used for modeling breaking waves, utilizing breaking criteria [26] or automatically defining subdomains where specific models should be applied.

References

- [1] AISSIOUENE, N., BRISTEAU, M.-O., GODLEWSKI, E., AND SAINTE-MARIE, J. A combined finite volume - finite element scheme for a dispersive shallow water system. *Networks and Heterogeneous Media (NHM)* (Jan. 2016).
- [2] ANDRIANOV, N. Performance of numerical methods on the non-unique solution to the riemann problem for the shallow water equations. *International Journal for Numerical Methods in Fluids* 47, 8-9 (2005), 825–831.
- [3] AUDUSSE, E., BOUCHUT, F., BRISTEAU, M.-O., KLEIN, R., AND PERTHAME, B. A fast and stable well-balanced scheme with hydrostatic reconstruction for shallow water flows. *SIAM J. Sci. Comput.* 25, 6 (2004), 2050–2065.
- [4] BENJAMIN, T. B., BONA, J. L., AND MAHONY, J. J. Model equations for long waves in nonlinear dispersive systems. *Philosophical Transactions of the Royal Society of London. Series A, Mathematical and Physical Sciences* 272, 1220 (2024/01/23 1997), 47–78.

- [5] BESSE, C., GAVRILYUK, S., KAZAKOVA, M., AND NOBLE, P. Perfectly matched layers methods for mixed hyperbolic–dispersive equations. *Water Waves* 4, 3 (oct 2022), 313–343.
- [6] BOUCHUT, F. *Nonlinear stability of finite volume methods for hyperbolic conservation laws, and well-balanced schemes for sources*. Springer Science & Business Media, 2004.
- [7] BOUTIN, B., COQUEL, F., AND LEFLOCH, P. G. Coupling techniques for nonlinear hyperbolic equations. I. self-similar diffusion for thin interfaces. *Proceedings of the Royal Society of Edinburgh Section A: Mathematics* 141, 5 (2011), 921–956.
- [8] BOUTIN, B., COQUEL, F., AND LEFLOCH, P. G. Coupling techniques for nonlinear hyperbolic equations. III. the well-balanced approximation of thick interfaces. *SIAM Journal on Numerical Analysis* 51, 2 (2013), 1108–1133.
- [9] BOUTIN, B., COQUEL, F., AND LEFLOCH, P. G. Coupling techniques for nonlinear hyperbolic equations. IV. well-balanced schemes for scalar multi-dimensional and multi-component laws. *Mathematics of Computation* 84, 294 (jan 2015), 1663–1702.
- [10] BOUTIN, B., COQUEL, F., AND LEFLOCH, P. G. Coupling techniques for nonlinear hyperbolic equations. II. resonant interfaces with internal structure. *Networks & Heterogeneous Media* 16, 2 (2021), 283.
- [11] BRESCH, D., LANNES, D., AND MÉTIVIER, G. Waves interacting with a partially immersed obstacle in the boussinesq regime. *Analysis & PDE* 14, 4 (jul 2021), 1085–1124.
- [12] CAMASSA, R., AND HOLM, D. D. An integrable shallow water equation with peaked solitons. *Phys. Rev. Lett.* 71 (Sep 1993), 1661–1664.
- [13] CIENFUEGOS, R., BARTHÉLEMY, E., AND BONNETON, P. A fourth-order compact finite volume scheme for fully nonlinear and weakly dispersive Boussinesq-type equations. Part I: model development and analysis. *International Journal for Numerical Methods in Fluids* 51, 11 (2006), 1217–1253.
- [14] DUCHÊNE, V. *Many Models for Water Waves*. Habilitation à diriger des recherches, Université de Rennes 1, July 2021.
- [15] DURAN, A., AND MARCHE, F. Discontinuous-galerkin discretization of a new class of green-naghdi equations. *Communications in Computational Physics* 17, 3 (Mar 2015), 721–760.
- [16] FAVRIE, N., AND GAVRILYUK, S. A rapid numerical method for solving serre-green-naghdi equations describing long free surface gravity waves. *Nonlinearity* 30, 7 (2017), 2718.

- [17] FERNÁNDEZ-NIETO, E. D., PARISOT, M., PENEL, Y., AND SAINTE-MARIE, J. A hierarchy of dispersive layer-averaged approximations of Euler equations for free surface flows. *Communications in Mathematical Sciences* 16, 5 (2018), 1169–1202.
- [18] GERBEAU, J.-F., AND PERTHAME, B. Derivation of viscous saint-venant system for laminar shallow water; numerical validation. *Discrete and Continuous Dynamical Systems - Series B* 1, 1 (2001), 89–102.
- [19] GODLEWSKI, E., PARISOT, M., SAINTE-MARIE, J., AND WAHL, F. Congested shallow water model: roof modeling in free surface flow. *ESAIM: Mathematical Modelling and Numerical Analysis* 52, 5 (Sep 2018), 1679–1707.
- [20] GODLEWSKI, E., AND RAVIART, P.-A. *Numerical approximation of hyperbolic systems of conservation laws*, vol. 118 of *Applied Mathematical Sciences*. Springer-Verlag, New York, 1996.
- [21] GODLEWSKI, E., THANH, K.-C. L., AND RAVIART, P.-A. The numerical interface coupling of nonlinear hyperbolic systems of conservation laws : II. The case of systems. *ESAIM: Mathematical Modelling and Numerical Analysis* 39, 4 (2005), 649–692.
- [22] GÖZ, M. F., AND MUNZ, C.-D. *Approximate Riemann Solvers for Fluid Flow with Material Interfaces*. Springer Netherlands, Dordrecht, 1998, pp. 211–235.
- [23] GREEN, A. E., AND NAGHDI, P. M. A derivation of equations for wave propagation in water of variable depth. *Journal of Fluid Mechanics* 78, 2 (1976), 237–246.
- [24] GUERMOND, J., MINEV, P., AND SHEN, J. An overview of projection methods for incompressible flows. *Computer Methods in Applied Mechanics and Engineering* 195, 44 (2006), 6011 – 6045.
- [25] KAZAKOVA, M., AND NOBLE, P. Discrete transparent boundary conditions for the linearized green–naghdi system of equations. *SIAM Journal on Numerical Analysis* 58, 1 (2020), 657–683.
- [26] KAZOLEA, M., DELIS, A., AND SYNOLAKIS, C. Numerical treatment of wave breaking on unstructured finite volume approximations for extended boussinesq-type equations. *Journal of Computational Physics* 271 (2014), 281–305. *Frontiers in Computational Physics*.
- [27] KAZOLEA, M., AND RICCHIUTO, M. Full nonlinearity in weakly dispersive boussinesq models: Luxury or necessity. *Journal of Hydraulic Engineering* 150, 1 (Jan. 2024).
- [28] KORTEWEG, D. J., AND DE VRIES, G. Xli. on the change of form of long waves advancing in a rectangular canal, and on a new type of long stationary waves. *The London, Edinburgh, and Dublin Philosophical Magazine and Journal of Science* 39, 240 (May 1895), 422–443.

- [29] LANNES, D. *The water waves problem: mathematical analysis and asymptotics*, vol. 188. Mathematical Surveys and Monographs, 2013.
- [30] LANNES, D., AND ALVAREZ-SAMANIEGO, B. A Nash-Moser theorem for singular evolution equations. Application to the Serre and Green-Naghdi equations. *Indiana Univ. Math. J.* 57 (2008), 97–132.
- [31] LANNES, D., AND MARCHE, F. A new class of fully nonlinear and weakly dispersive Green–Naghdi models for efficient 2D simulations. *Journal of Computational Physics* 282 (2 2015), 238–268.
- [32] LANNES, D., AND RIGAL, M. General boundary conditions for a boussinesq model with varying bathymetry. *Work in progress*.
- [33] LANNES, D., AND WEYNANS, L. Generating boundary conditions for a boussinesq system. *Nonlinearity* 33, 12 (oct 2020), 6868–6889.
- [34] LEVEQUE, R. J. *Finite volume methods for hyperbolic problems*, vol. 31. Cambridge university press, 2002.
- [35] LI, M., GUYENNE, P., LI, F., AND XU, L. High order well-balanced cdg-fe methods for shallow water waves by a green–naghdi model. *Journal of Computational Physics* 257 (2014), 169 – 192.
- [36] MADSEN, P. A., AND SCHÄFFER, H. A. Higher–order boussinesq–type equations for surface gravity waves: derivation and analysis. *Philosophical Transactions of the Royal Society of London. Series A: Mathematical, Physical and Engineering Sciences* 356, 1749 (2022/03/16 1998), 3123–3181.
- [37] MATSUNO, Y. Hamiltonian formulation of the extended green–naghdi equations. *Physica D: Nonlinear Phenomena* 301-302 (2015), 1–7.
- [38] MITSOTAKIS, D., ILAN, B., AND DUTYKH, D. On the galerkin/finite-element method for the serre equations. *Journal of Scientific Computing* 61, 1 (Feb 2014), 166–195.
- [39] NOELLE, S., PARISOT, M., AND TSCHERPEL, T. A class of boundary conditions for time-discrete Green-Naghdi equations with bathymetry. *SIAM Journal on Numerical Analysis* (2022).
- [40] PARISOT, M. Entropy-satisfying scheme for a hierarchy of dispersive reduced models of free surface flow. *International Journal for Numerical Methods in Fluids* 91, 10 (2019), 509–531.
- [41] PEREGRINE, D. H. Long waves on a beach. *Journal of Fluid Mechanics* 27, 04 (1967), 815–827.
- [42] RICCHIUTO, M., AND FILIPPINI, A. Upwind residual discretization of enhanced boussinesq equations for wave propagation over complex bathymetries. *Journal of Computational Physics* 271 (2014), 306 – 341. *Frontiers in Computational Physics*.

- [43] TORO, E. F. *Riemann solvers and numerical methods for fluid dynamics: a practical introduction*. Springer Science & Business Media, 2013.
- [44] WEI, G., KIRBY, J. T., AND SINHA, A. Generation of waves in boussinesq models using a source function method. *Coastal Engineering* 36, 4 (1999), 271–299.
- [45] YAMAZAKI, Y., KOWALIK, Z., AND CHEUNG, K. F. Depth-integrated, non-hydrostatic model for wave breaking and run-up. *International Journal for Numerical Methods in Fluids* 61, 5 (2009), 473–497.